PHYSICAL MODELING OF DRUG TRANSPORT IN CANCER

by

Şirin Yonucu

M.Sc., Physics, Boğaziçi University, 2012,

B.S., Physics, Boğaziçi University, 2009

Submitted to the Institute for Graduate Studies in
Science and Engineering in partial fulfillment of
the requirements for the degree of
Doctor of Philosophy

Graduate Program in Physics
Boğaziçi University
2018

PHYSICAL MODELING OF DRUG TRANSPORT IN CANCER

APPROVED BY:

Prof. Mehmet Burcin Ünlü .....
(Thesis Supervisor)

Prof. Mehmet Naci İnci .....

Prof. Mehmet Levent Kurnaz .....

Assoc. Prof. Savaş Arapoğlu .....

Prof. Yavuz Ekşi .....

DATE OF APPROVAL: 02.08.2018

ACKNOWLEDGEMENTS

Firstly, I would like to express my sincere gratitude to my advisor Prof. Mehmet Burçin Ünlü for the continuous support of my Ph.D study and related research, for his patience, motivation, and immense foresight. His guidance helped me in all the time of research and writing of this thesis.

Besides my advisor, I would like to thank the rest of my thesis committee: Prof. Mehmet Naci İnci, Prof. Mehmet Levent Kurnaz, Prof. Yavuz Ekşi, and Assoc. Prof. Savaş Arapoğlu, for their insightful comments and encouragement, contributing to my graduation.

My sincere thanks go to Prof. Mohammad Kohandel, who guided me to lay the foundations of this work and helped me in the way with great kindness and patience. I also would like to thank Dr. Colin Phipps and Defne Yılmaz for their exceptional contributions to my work. Without their precious support, it would not be possible to conduct this research.

I thank my fellow lab mates and dear friends Irem Demirkan, Nasire Uluç, Aytaç Demirkıran, Mert Tuzer, Gizem Alpakut, Uğur Parlatan and Seydi Yavaş. Seeing their smiling faces every day was more than enough to motivate me.

Last but not the least, I would like to thank my late parents, Kenan Yonucu and Fatma Yılmaz, my dear sister and lifelong supporter Ayşegül Yonucu, and finally my life companion Bora Ünver who is more than family to me.

ABSTRACT

PHYSICAL MODELING OF DRUG TRANSPORT IN CANCER

Understanding the interaction of tumors with their microenvironment is imperative to understand its development and to increase the efficiency of therapies. In addition to all other genetic and biochemical determinants of tumor system that make it very different than healthy tissue, morphological properties of tumor system and resulting physical properties add to this difference creating strong contrasts compared to its healthy counterpart. Therefore, examining the physics of this system is an important part of cancer research. In this work, we delve into the physics of tumor and its blood vessels to understand its role in tumor growth and response to therapy. We tried to resolve the physical problem of transport of drugs to tumor microenvironment efficiently. To achieve that, we created a tumor simulator by building a mathematical model framework that includes spatial representations of tumors and their microenvironment. Since vessels are the distributors of drugs and they are responsible for abnormal fluid flow, and resultant changes in fluid pressure, treatments manipulating tumors vessels were explored to enhance drug delivery. Specific models are built for simulating normalization of tumor blood vessels and promoting vessel growth with different treatments. These two approaches are tried using different doses of drug combinations and drug scheduling to optimize the benefit from chemotherapy. For each case, we revealed the advantages and disadvantages of these approaches and the physical reasons behind them.

ÖZET

KANSERDE İLAÇ TAŞINMASININ FİZİKSEL MODELİ

Tümörlerin mikroçevreleri ile etkileşimini anlamak, tümor gelişimini anlamak ve tedavilerin etkinliğini arttırmak için zorunludur. Tümör sisteminin sağlıklı dokudan çok farklı kılan tüm diğer genetik ve biyokimyasal belirleyicilere ek olarak, tümör sisteminin morfolojik özellikleri ve sonuçta ortaya çıkan fiziksel özellikler, sağlıklı muadillerine göre güçlü kontrastlar yaratır. Bu nedenle bu sistemin fiziğini incelemek, kanser araştırmalarının önemli bir parçasıdır. Bu çalışmada tümör büyümesi ve tedaviye yanıt üzerindeki rolünü anlamak için tümör ve kan damarlarının fiziğine başvurduk. İlaçların tümör mikroçevresine etkili bir şekilde taşınmasıyla ilgili fiziksel problemi çözmeye çalıştık. Bunu başarmak için, tümörün ve mikroçevresinin mekansal temsillerini içeren bir matematiksel model çerçevesi oluşturarak bir tümör simülatörü yarattık. Damarlar ilaçların dağıtıcısı olduğundan ve anormal sıvı akışından ve sıvı basıncında ortaya çıkan değişikliklerden sorumlu oldukları için, ilaç dağıtımını geliştirmek için tümör damarlarını manipüle eden tedaviler araştırılmıştır. Tümör kan damarlarının normalleşmesini simüle etmek ve farklı tedavilerle damar büyümesini teşvik etmek için özel modeller üretilmiştir. Bu iki yaklaşım, kemoterapinin faydasını optimize etmek için farklı ilaç kombinasyonları ve ilaç programlaması kullanılarak denenmiştir. Her vaka için bu yaklaşımların avantaj ve dezavantajları ve bunların arkasındaki fiziksel nedenler ortaya çıkarılmıştır.

TABLE OF CONTENTS

ACKNOWLEDGEMENTS iii
ABSTRACT iv
ÖZET v
LIST OF FIGURES viii
LIST OF TABLES x
LIST OF SYMBOLS xi
LIST OF ACRONYMS/ABBREVIATIONS xiv
1. INTRODUCTION 1
1.1. Thesis Outline 3
2. BIOLOGICAL BACKGROUND 4
2.1. Tumor Growth 6
2.2. Angiogenesis 8
2.3. Tumor Microenvironment 10
2.4. Cancer Therapies 10
2.4.1. Chemotherapy 12
2.4.2. Therapies Targeting Tumor Vessels 13
2.5. Drug Delivery in Tumors 16
3. DEVELOPEMENT OF TUMOR GROWTH AND TREATMENT RESPONSE MODEL 19
3.1. Tumor Growth 19
3.2. Vessel Growth 21
3.3. Interstitial Fluid Pressure 23
3.4. Generalized Drug Equation 26
3.5. Solution Method 29
4. EFFECT OF NORMALIZATION IN CHEMOTHERAPY DELIVERY AND RESPONSE 34
4.1. Related Literature Review in Modeling of Tumor 36
4.2. Mathematical Model 37
4.3. Model Equations 38

4.3.1. Tumor cells, vasculature and IFP 38
4.3.2. Antiangiogenic agent and chemotherapy drug 41
4.4. Results 43
4.5. Discussion 50
5. PROANGIOGENIC TREATMENT STRATEGIES TO ENHANCE DRUG DELIVERY AND TREATMENT RESPONSE 56
5.1. Related Literature Review in Modeling of Tumor 58
5.2. Mathematical Model 59
5.3. Model Equations 60
5.3.1. Tumor cells, vasculature, and IFP 60
5.3.2. Proangiogenic and chemotherapy drugs 62
5.4. Results 64
5.5. Discussion 69
6. CONCLUSION 72
REFERENCES 74

LIST OF FIGURES

Figure 2.1. Representation of a typical tissue showing epithelial and mesenchymal components 4

Figure 2.2. Hallmarks of cancer 5

Figure 2.3. Effects of hypoxia and acidosis on tumors 7

Figure 2.4. Abnormal vessel created by angiogenesis 9

Figure 2.5. IFP maps and profiles of tumors composed of typical Human NCI-H460 non–small-cell lung cancer cells on mice 11

Figure 2.6. Developement of internal resistance to chemotherapy. 13

Figure 2.7. Effects of therapies manipulating tumor vessels 15

Figure 2.8. Transport in tumor microenvironment 18

Figure 3.1. Tumor growth in simulations. 21

Figure 3.2. Vessel growth in simulations. 22

Figure 3.3. A simple compartment PK model for drug delivery in the tumor. . 27

Figure 3.4. PK/PD models to analyze drug delivery and response 28

Figure 3.5. Spatial computational domain. 31

Figure 4.1. Control case showing vessel and tumor densities and IFP for days 19, 23 and 27. 44

Figure 4.2. Drug regimens. 45

Figure 4.3. Tumor density and chemotherapy drug extravasation coefficient. . 47

Figure 4.4. Average IFP over whole tumor and average cell density in the interior region of tumor. 49

Figure 4.5. Drug extravasation rate from vessels and total drug exposure per unit area in the interior region of tumor by the end of the simulation. 49

Figure 4.6. Tumor density and chemotherapy drug extravasation coefficient for drugs acting on tumor cell proliferation. 51

Figure 5.1. Tumor cell and vessel density for tumors with high vessel density. 66

Figure 5.2. Tumor cell and vessel density for tumors with low vessel density. 67

Figure 5.3. Total number of tumor cells in time. 68

Figure 5.4. IFP along the radius of tumor. 68

LIST OF TABLES

Table 3.1. Models explaining tumor growth 20

Table 4.1. Interstitial fluid transport parameters. 40

Table 4.2. Parameters related to transport of 100 nm liposomes and antiangiogenic agents. 42

Table 5.1. Dimensionless tumor and vessel growth parameters. 62

Table 5.2. Transport parameters of small chemotherpy drug Doxorubicin. . . 63

Table 5.3. Proangiogenic drugs and chemotherapy combinations. 65

LIST OF SYMBOLS

a	Sigmoid growth exponent
A	Concentration of antiangiogenic agent
A_0	Peak plasma concentration of angiogenic agents
A_r	Reaction coefficient between vessels and antiangiogenic agent
A_v	Plasma antiangiogenic agent concentration
A_V	VEGF production coefficient from proangiogenic agent
b	Sigmoid decay exponent
d	Concentration of chemotherapy drug
d_0	Peak plasma concentration of chemotherapy drugs
D_A	Diffusion coefficient of antiangiogenic agent
D_d	Diffusion coefficient of chemotherapy drug
d_i	Chemotherapy drug concentration
D_i	Diffusion coefficient of chemotherapy drug
d_{ir}	Reaction coefficient between tumor cells and chemotherapy drug
D_m	Diffusion coefficient for vessels
d_{max}	Maximum chemotherapy drug concentration that extravasated inside the tumor
d_n	Reaction coefficient between tumor cells and chemotherapy drug
D_n	Diffusion coefficient for tumor cells
d_r	Rate of chemotherapy drug elimination as a result of reaction with tumor cells
d_v	Plasma chemotherapy drug concentration
d_v^i	Plasma chemotherapy drug concentration
g_v	VEGF production coefficient
h	Incremental change
H_n	Hydraulic conductivity of normal vessels
K	Hydraulic conductivity of the interstitium

k_λ	Hydraulic conductivity increase rate from proangiogenic agent
k_A	Decay rate of antiangiogenic agents
k_d	Decay rate of chemotherapy drugs
k_E	Retardation coefficient for interstitial convection
k_i	Decay of chemotherapy drugs
k_v	VEGF decay
L_p	Hydraulic conductivity of vessel wall
m	Vessel density
m_{max}	Maximum vessel density
n	Tumor cell density
n_{lim}	Carrying capacity for tumor cell density
p	Tumor cell population
P	Interstitial fluid pressure
P_0	Interstitial fluid pressure in normal tissue
P_v	Vascular pressure
Q	Axial blood flow in vessels
r	Tumor cell density growth rate
r_m	Vessel decay coefficient
S/V	Vessel surface density
u	Function
$\mathbf{u}$	Interstitial fluid flow
$t^A_{1/2}$	Plasma half-lives of the antiangiogenic agent
$t^d_{1/2}$	Plasma half-lives of the chemotherapy drugs
V	VEGF concentration
α	First coefficient for vessel growth
α_{mn}	Coupling coefficient for tumors with vessels
α_{nm}	Angiogenesis production coefficient
α'_{nm}	Angiogenesis production coefficient
β	Second coefficient for vessel growth
β_{nm}	Angiogenesis dispersion coefficient

β'_{nm}	Angiogenesis dispersion coefficient
γ	Third coefficient for vessel growth
Γ_b	Supply of the fluid from blood vessels into the interstitial space
Γ_ℓ	Fluid drainage from the interstitial space into the lymph vessels
η	Blood viscosity
κ	Growth rate
κ_1	Sigmoid growth rate
κ_2	Sigmoid decay rate
λ_A	Transvascular diffusion coefficient of antiangiogenic agents
λ_b	Hydraulic conductivities of blood vessels
λ_i	transvascular diffusion coefficient of chemotherapy drug
λ_ℓ	Hydraulic conductivities of lymphatics
π_c	Capillary oncotic pressure
π_i	Interstitial oncotic pressure
ρ	Vessel diameter
σ_d	Solvent drag reflection coefficient
σ_i	Solvent drag reflection coefficient
σ_v	Osmotic reflection coefficient

LIST OF ACRONYMS/ABBREVIATIONS

2-D	Two Dimensional
3-D	Three Dimensional
Ang	Angiopoietin
DNA	Deoxyribonucleic Acid
ECM	Extracellular Matrix
EPR	Enhanced Permeability and Retention Effect
G_1	Gap 1
G_2	Gap 2
IF	Interstitial Fluid
IFP	Interstitial Fluid Pressure
LD	Large Drug
M	Mitotic
MVD	Microvessel Density
MVP	Microvascular Pressure
ODE	Ordinary Differential Equation
PD	Pharmacodynamic
PDE	Partial Differential Equation
pH	Acidity
PK	Pharmacokinetic
RGD	Arginylglycylaspartic Acid
S	Synthesis
SD	Small Drug
VEGF	Vascular Endothelial Growth Factor
VEGFR-2	Vascular Endothelial Growth Factor Receptor 2

1. INTRODUCTION

Although cancer is a disease that initiated by changes in genes, more and more evidence appear every day about the fact that understanding the genes involving in the process is not enough for understanding cancer and to find ways to battle it. Cancer is now viewed as a complex disease whose development depends on the interaction of genes and its microenvironment including biochemicals and even physical forces.

Due to its complex nature, understanding cancer requires combined efforts of many disciplines. There are many physical aspects to tumor growth. Tumor cells reproduce avoiding population control mechanisms acting on healthy cells [1]. Overpopulation of tumor cells causes the solid pressure increase, irregular and leaky tumor vessels increases fluid pressure inside the tumors [2]. These abnormalities lead to changes in fluid movement from vessels to tumors and within the tumors compared to healthy tissue. The physical changes in microenvironment complicate the treatment process. Therefore, the efficient delivery of drugs to tumors cells constitutes a physical problem.

In this thesis, we explore the tumor growth in relation to its microenvironment, approaching them as a physical system. Tumor cells and vessels are modeled using partial differential equations for the development of multiscale spatiotemporal tumor simulator. Tumor vessels are modeled such that they evolve according to the interactions with tumor cells, initiate angiogenesis which is the production of new vessels, and reach to a configuration which is observed in real tumors. vessel structure is composed of heterogeneously distributed vessel islands due to these interactions. Tumor cells also interact with vessels increasing the growth rate of the tumor. The model has equations accounting for the transport of fluid from vessels to tissue and back to the lymph system. We calculate the interstitial fluid velocity field and interior pressure of the tumor by quantifying this fluid transport. There is also representation of a lymph system in the model.

We use the tumor cells, vessels and interstitial fluid pressure (IFP) framework to simulate drug treatments. We evaluate the delivery of the drugs and using different treatment types, dosage and schedule to observe treatment results in our simulations. This framework replicates the physical delivery barriers posed on the tumor by microenvironmental abnormalities seen commonly in tumors. Simulation results enable us to see the nonlinear effects created by tumor microenvironment and by drug therapy.

We utilize this system to evaluate combination therapies of antiangiogenic agents (drugs that inhibits new vessel formation) with chemotherapy. We observe the particular results in each kind of treatment exploring the problems about them and optimize them regarding enhancing and homogenizing drug delivery through the tumor and minimizing the tumor size.

We use this simulator to explore normalization of tumor vessels which is a process making leaky and irregular blood vessels to turn into less leaky, regular and functional vessels that resemble the vessels in the healthy tissue [2,3]. The process which is induced by the application of antiangiogenic agents is studied concerning its benefit in reducing IFP and enhancing drug delivery. The ultimate treatment response after chemotherapy application with normalized tumor vessels is evaluated. A drug scheduling for combination therapy is proposed to obtain a more homogeneous chemotherapy delivery and decreased tumor cell density within the tumor compared to the only chemotherapy applications.

Another phenomenon concerning tumor vessels, vascular promotion is also studied using tumor growth simulator. Vascular promotion is achieved through the application of a low dose of some antiangiogenic agents to the tumor, increasing vessel density and leakiness [4]. This time, the unfavorable result for drug delivery, the increase in IFP is balanced with a beneficial increase in vessel density regarding drug delivery to create best-case scenarios with this combination therapy. Properties of chemotherapy drugs best fitted to this combination therapy to yield drug delivery benefit and better treatment response are studied compared to only chemotherapy applications.

1.1. Thesis Outline

In Chapter 2, the relevant biological background for tumor growth, angiogenesis and tumor microenvironment is given. Cancer therapies are generally explained, and chemotherapy and therapies targeting tumor vessels are studied. Problems about drug delivery in the tumor microenvironment are addressed in detail.

In Chapter 3, the development of multiscale spatiotemporal tumor growth and drug response model is explained. Base equations for model components: tumor cell density, vessel density, interstitial fluid pressure and a generalized equation for drugs are derived. Solution method and algorithm is discussed.

In Chapter 4, based on the model framework given in Chapter 3, a specialized model is built for assessment of vascular normalization in the context of its benefit on drug delivery and treatment response. Simulation results are given to show the optimal conditions for that therapy, and its effect on the spatial distribution of chemotherapy drugs.

In Chapter 5, based on the model framework given in Chapter 3, a specialized model is built for assessment of vascular promotion in the context of its benefit on drug delivery and treatment response. Simulation results are given to show the optimal conditions for that therapy, and the properties of the chemotherapy drugs best suited for this type of therapy are suggested.

In Chapter 6, a conclusion for the thesis is constructed explaining the most critical results given by the physical models of tumor studied here.

2. BIOLOGICAL BACKGROUND

Tumor cells can be described as cells escaping from normal control mechanisms [5, 6]. A series of mutations need to occur in cells to enable this transition and tumor appear as a mass of differently mutated cells [6]. The balance between proliferation, death, and differentiation ensure that cell number remains constant in healthy tissue. This balance is broken through in tumors by increased cell number arising either from blocked death and/or differentiation or increased proliferation with no change in the other two properties [7].

Tumors can be divided into three groups as benign, *in situ*, and cancers [5]. Benign tumors can appear in any tissue growing in and damaging the tissue locally without spreading to distant locations. *In situ* tumors are mostly small tumors usually appearing and staying in epithelium without moving through the basement membrane and supporting mesenchyme. Figure 2.1 of a typical tissue shows these components. Epithelium layers outer surfaces of organs and blood vessels and inner surfaces of cavities of many organs. Cancers are malignant tumors that have the capacity for local invasion. It is a large group of diseases having more than two hundred distinct types.

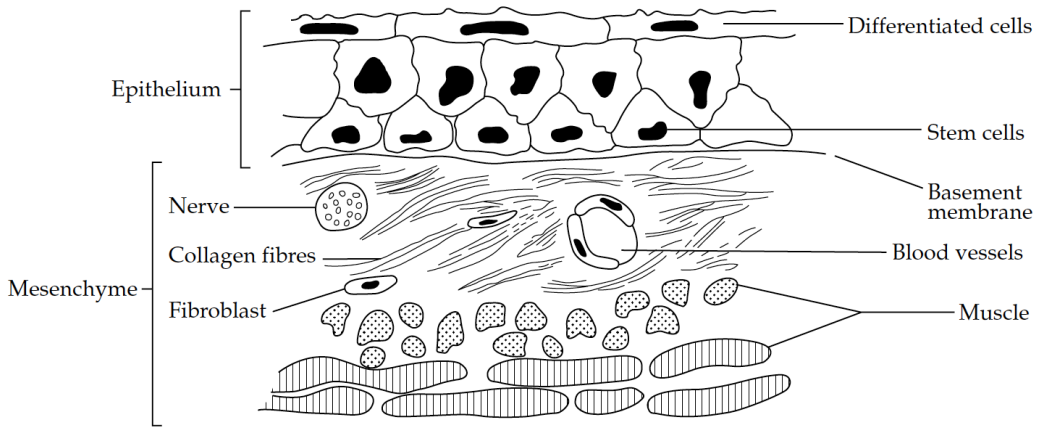

Figure 2.1. Representation of a typical tissue showing epithelial and mesenchymal components [5].

Transformation of normal cells is called tumorigenesis which is a multi-step process of genetic alterations. Hanahan and Weinberg identified eight commonly appearing alterations in cancer cells as self-sufficiency in growth signals, insensitivity to growth-inhibitory signals, evasion of programmed cell death, limitless replicative potential, sustained angiogenesis, and tissue invasion and metastasis in their article published in 2000 [1]. They added two additional emerging hallmarks and two enabling characteristics to this work in 2011 to complete the picture of malignant transformation [8]. Figure 2.2 shows all hallmarks including the new additions; reprogramming energy metabolism, evading immune destruction, genome instability and mutation, and tumor-promoting inflammation.

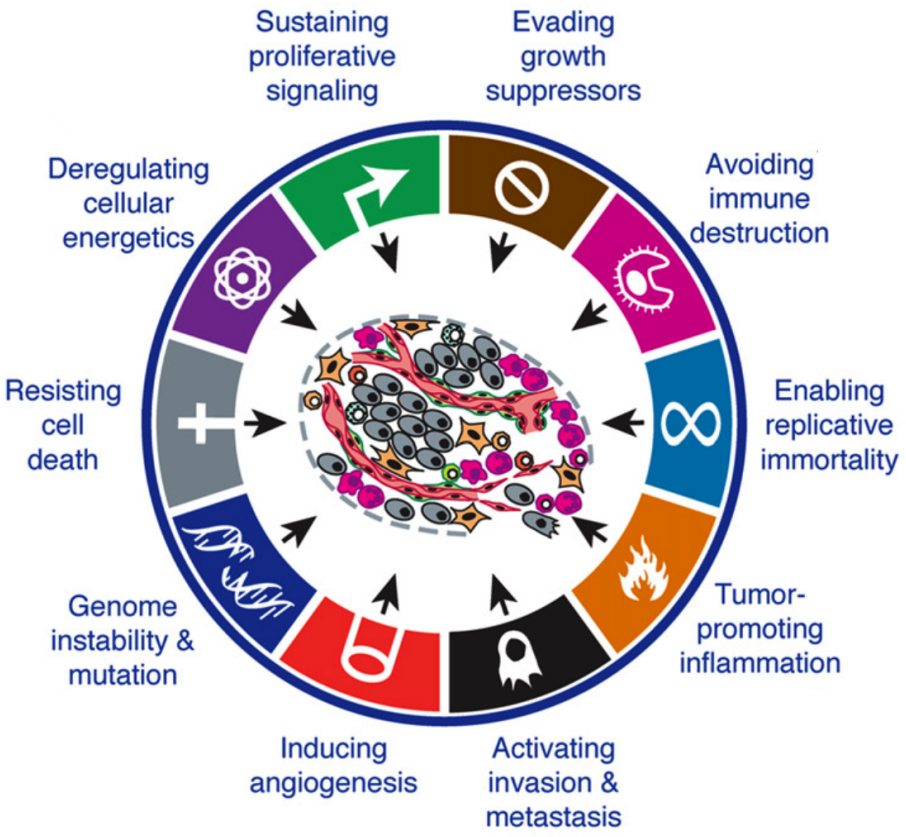

Figure 2.2. Hallmarks of cancer [8].

2.1. Tumor Growth

Dividing cells in body pass through a series of stages making up cell cycle, in which two daughter cells produced from one dividing cell. Cell cycle completes in two phases called interphase and mitotic phase. Interphase begins with G_1 phase in which the cell grows, copies organelles, and makes the molecules to prepare for later steps. Next comes the S phase, in which the cell produce a complete copy of the DNA and duplicates the centrosome which helps to separate DNA during M phase. Interphase is completed by the end of G_2 phase in which cell grow further, produces proteins and organelles and rearrange its contents for preparation of mitosis. The mitotic phase includes the separation of DNA into two sets and division of cells cytoplasm, finally forming two new cells. Several checkpoints regulate the proliferation during cell cycle whose failures results in uncontrolled growth. Cell death can occur passively by necrosis or in a programmed manner with the synthesis of macromolecules by apoptosis [7]. Tumor cells usually accumulate mutations on the genes that have potential to cause cancer (oncogenes) and genes that prevents a cell from becoming cancerous (tumor suppressor genes) [9] which help them to evade control mechanisms that induce apoptosis [1]. Proliferation rate is similar for mutated cells and host cells. Since tumor cells do not have population control mechanisms, cell density increases in the tumor microenvironment. As tumor cells continue to be differentiated this rate also changes making doubling times faster for metastases than primary tumors [7].

The inherent vasculature is not able to sustain tumors growing beyond $1mm^3$ regarding nutrient and oxygen and at this stage and tumor size is limited to diffusion from vessels which are about $100 - 200\mu m$ [9]. Due to excess in proliferation, cells in tumor center that are devoid of nutrients and oxygen start to go through necrotic cell death composing a necrotic core. Between highly proliferating outer rim and necrotic core, oxygen drops below to required levels to sustain cell metabolism which is called hypoxia. High consumption of oxygen by tumor cells creates chronic hypoxia by limiting diffusion length from available vessels (diffusion limited delivery), and lack of vessels or blood perfusion in the region creates acute hypoxia (perfusion limited delivery) [10].

Hypoxia triggers changes from aerobic to anaerobic metabolism [10, 11]. This metabolic shift results in acidic extracellular pH. Acidosis also appears when there is oxygen in the extracellular region, this tendency of tumor cells are called "the Warburg effect" [12]. These microenvironmental factors lead to evasion of the immune system, increase in invasive and metastatic potential and creation of selective survival pressures for cancer cells to adapt [13]. Hypoxia also triggers a switch mechanism for blood vessel production called angiogenesis. During angiogenesis, vascular endothelial growth factors (VEGF) activate the receptors on endothelial cells in existing vessels for sprouting of new vessels. By recruiting their blood supply, tumors can grow beyond $1-2mm$ in diameter [5]. However, as tumors grow, vessels remain insufficient to sustain tumors due to unfunctional nature of vessels produced by angiogenesis and vascular collapse due to increased solid and fluid pressure building up inside the tumors [2]. Therefore, hypoxia is not fully evaded after the angiogenic switch. Consequences of hypoxia and acidosis are summarized in Figure 2.3.

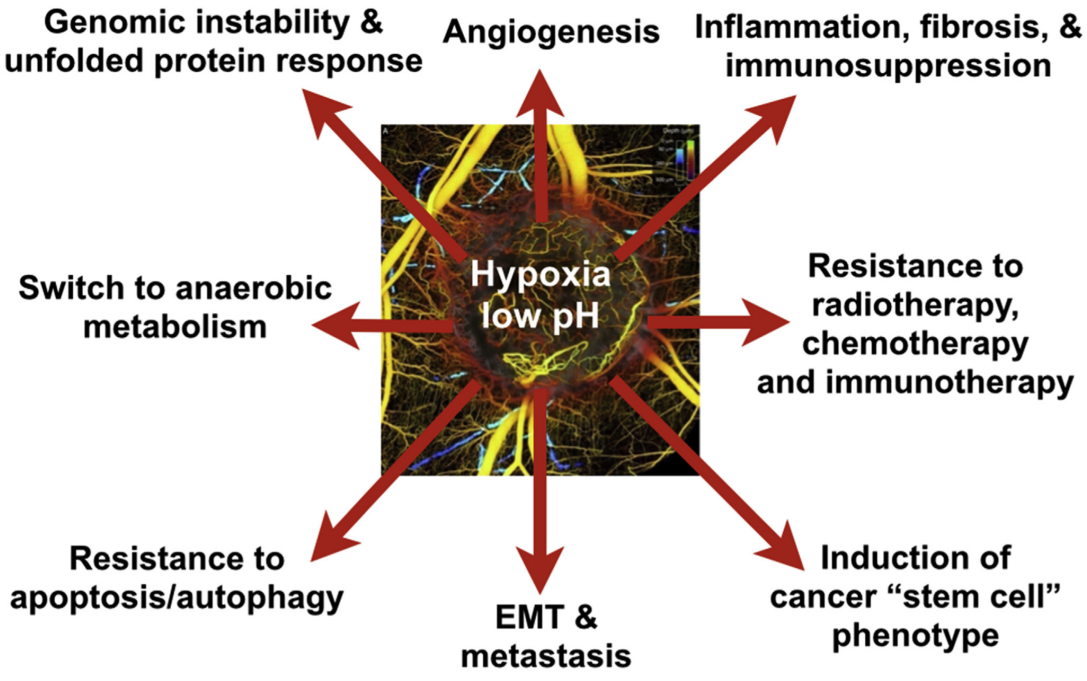

Figure 2.3. Effects of hypoxia and acidosis on tumors [13].

By the support of the new vessels produced with angiogenesis, tumor begins to invade surrounding host tissue. Tumor cells can spread via blood or lymph vessels and body cavities to a different location resulting in the formation of a new tumor in the host body which is called metastasis [7]. Metastasis is found to be highly correlated with vascularity of tumors and angiogenesis [14].

2.2. Angiogenesis

Angiogenesis which is utilized by tumors to obtain blood supply is a restricted process after embryonic development. It is activated only during the female reproductive cycle, wound healing, and in certain diseases and cancer [5]. Pro and antiangiogenic factors are in balance in normal conditions, tumors initiate production of proangiogenic factors like vascular endothelial growth factor (VEGF), triggering the angiogenic switch mechanism. Angiogenesis in tumor produces unfunctional vessels since it lacks control mechanisms acting on the angiogenesis in normal tissue [11, 13].

Angiogenesis starts with degradation of the capillary basement membrane and the local extracellular matrix. Endothelial cells are activated and migrated towards the angiogenic stimulus. They proliferate at a rate 50–200 times greater than their healthy counterparts and differentiate forming new vessels. Proliferation mainly occurs in tumor periphery and microvessel density (MVD) is four to ten times greater in periphery than in the interior regions [15].

The tumor vessels produced by angiogenesis have morphological changes as shown in Figure 2.4. Incomplete support from pericytes and a basement membrane makes them leaky compared to normal vessels [5, 9]. Vessels have abnormal branching; they form sinusoids and arteriovenous shunts [15]. The resulting vasculature is very heterogeneous and insufficient in terms of supplying blood. As a result of abnormal vascular structure in tumors, hypoxia and high acidity remain as a problem even after the angiogenic switch.

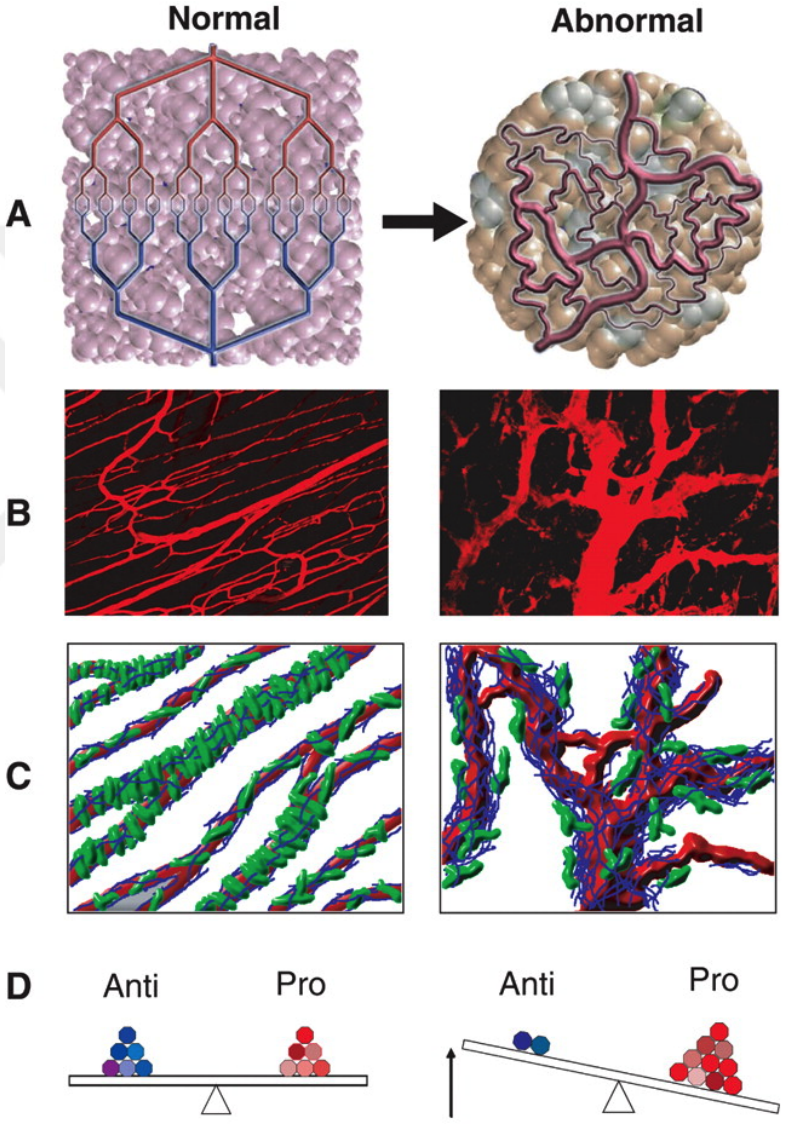

Figure 2.4. Abnormal vessel created by angiogenesis [2].

2.3. Tumor Microenvironment

Tumor cells are embedded in a fibrous structure called extracellular matrix (ECM) surrounded by interstitial fluid (IF) which is circulating between vessels, ECM and lymph vessels. Within ECM, fibroblasts, myofibroblasts, endothelial cells reside making up the tumor stroma [16].

IF carries nutrients and other micro and macromolecules necessary for the homeostasis of the system. Degradation of ECM takes place during pathogenesis and tumor cell proliferation. After degradation, ECM is build up again by tumor cells. This remodeled tumor ECM is different from that of normal inherent tissue [16, 17]. It is stiffer due to increased pressure from rapid proliferation [9].

Aside from hypoxia, abnormal vessels produced by angiogenesis generate other abnormalities in tumor microenvironment. Due to the large holes in capillary walls, fluid exit from vessels in higher amounts compared to normal tissue. As fluid accumulate extracellular region of tumors, interstitial fluid pressure (IFP) builds up inside the tumors [9]. In the meantime, increased solid pressure collapses lymph vessels in the interior regions of tumor [18]. These factors create a common IFP profile observed in solid tumors with an elevated plateau in the central region which drops sharply to normal tissue IFP levels at tumor boundary [19, 20]. Figure 2.5 shows IFP maps and profiles of tumors composed of typical Human NCI-H460 non–small-cell lung cancer cells in mice [21]. In some cases, IFP is found to be as high as microvascular pressure (MVP) inside tumors preventing any fluid transport from vessels.

2.4. Cancer Therapies

For solid tumors, the initial step of the therapy is surgical removal of the tumor with a margin of healthy tissue since the surface of tumors are usually irregular [7]. Starting with adjuvant therapy after the surgery is common [5, 7].

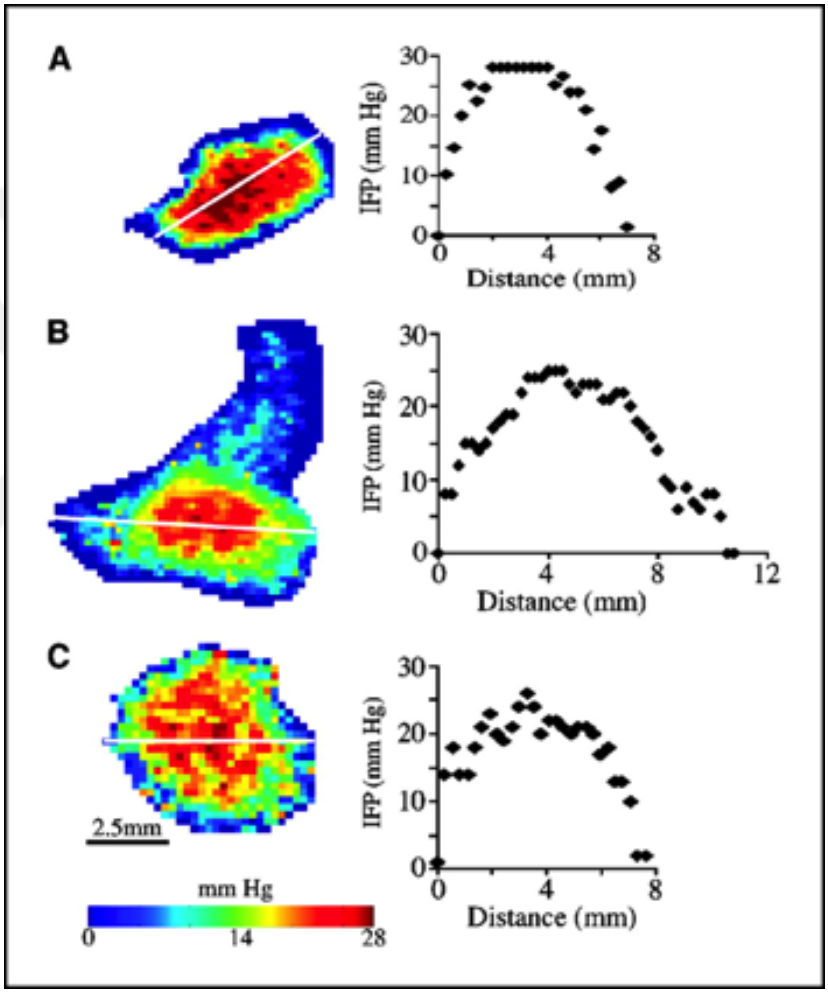

Figure 2.5. IFP maps and profiles of tumors composed of typical Human NCI-H460 non–small-cell lung cancer cells on mice [21].

Adjuvant therapy aims to clear the body from remaining tumor cells. It can involve radiotherapy and chemotherapy. When anatomy of tumor site is complex like brain and spine, radiotherapy is preferred as initial action [7]. Radiotherapy aims to kill tumor cells by damaging their DNA. Dividing cells are more sensitive to radiotherapy; hence, radiotherapy dose is fractioned to catch tumor cells in different stages in cell cycles [7]. In some cases, neoadjuvant therapy is applied before surgery by chemotherapy radiotherapy or hormone therapy to make tumor operable.

2.4.1. Chemotherapy

Chemotherapy mainly consists of cytotoxic drugs which act on tumor DNA and processes related to DNA [5]. Since these drugs also affect healthy cells dosing should be carefully determined to minimize the side effects. Drugs designed in a way to exploit differences in their cellular ability to repair damage in tumorous and healthy tissue. Therefore, drug scheduling takes into account the time required for healthy cells to repair themselves in between each chemotherapy application [5]. In addition to cytotoxic drugs, cytostatic drugs which inhibits tumor growth also used in combination with other therapies.

Drugs must be delivered in sufficient concentrations and duration of exposure to kill the tumor cells successfully [7]. Since tumor vasculature is very heterogeneous spatially and in terms of perfusion, tumor cells that far away from vessels are not exposed to drugs. Not reaching to tumor cells or other external factors create extrinsic resistance. In addition to that, not every tumor cell dies even though they are exposed to drugs, they may already have or develop internal resistance during therapy [7]. When resistance occurs, the tumor may have limited response or regrow after the initial treatment. The regrowing population is mostly composed of resistant cells [5].

Pharmacokinetic models are used to maximize the effects of treatment. They are mathematical models to calculate the amount of drugs reaching tumor cells, their metabolism, absorption, and excretion regarding different routes of administration.

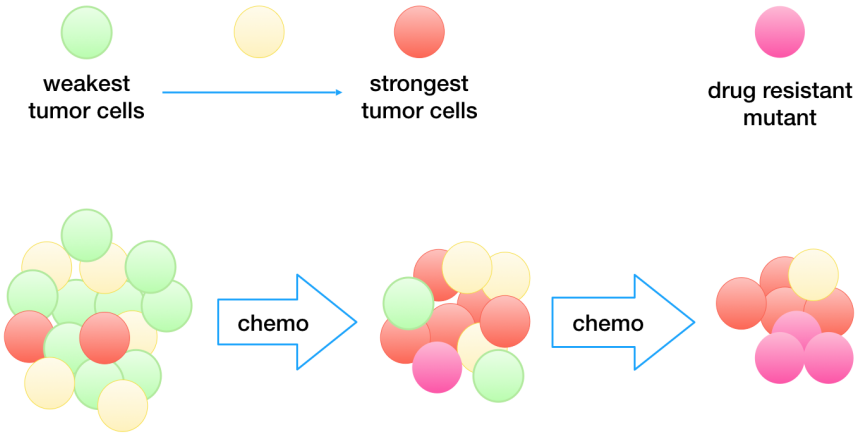

Figure 2.6. Developement of internal resistance to chemotherapy.

Due to the heterogeneity of tumors, pharmacokinetic studies more frequently correlates with toxicity rather than drug efficiency [5].

2.4.2. Therapies Targeting Tumor Vessels

Ever since tumor growth is found to be tightly dependent on initiation of angiogenesis, it became a target for therapy. Inhibiting angiogenesis to starve tumors was the first purpose of drugs targeting angiogenesis [13].

Antiangiogenic agents which inhibit angiogenesis are produced for that reason, however, they are not adequate for reducing tumor size when applied alone [13]. They are usually combined with chemotherapy and radiotherapy for enhancing the effect of therapy. Effect of angiogenesis on killing tumor cells is based upon the fact that necrosis occurs beyond diffusion length which corresponds to about $150\mu m$ radius surrounding blood vessels [7]. Clinical use of antiangiogenic agents did not replicate the success they show in animal models [22]. When they are used in combination with other therapies, they were diminishing vessels and was starving tumors. On the other hand, they were hindering the delivery of chemotherapy and creating hypoxia which reduces the effectiveness of radiotherapy. Therefore, their use is a controversial subject.

The close observation of the activity of antiangiogenic drugs leads to the discovery of a new phenomenon called "vascular normalization." Antiangiogenic agents, when applied in controlled doses, is found to kill unfunctional part of the vasculature, increase the pericyte coverage to reduce leakiness enabling better blood perfusion in vessels [2,3]. Vessel density and leakiness are decreased resulting in a decrease in IFP. Normalization depends on the restoration of balance between pro and antiangiogenic agents in tumor microenvironment [2]. In healthy tissue they are already in balance, however, to initiate angiogenesis tumors produce proangiogenic factors like VEGF to disturb the balance. When the balance is reached again by the addition of antiangiogenic agents to the system, vascular normalization is induced. However, it is tough to attain that balance with externally given drugs. At some point during therapy, the excess of antiangiogenic agents tip the balance again in favor of vessel destruction, now starting to kill functional vessels. Therefore normalization is a transient process that needs to be carefully managed regarding drug dose and schedule to be actualized [23, 24]. Normalization of blood vessels also normalizes the tumor microenvironment by decreasing hypoxia and IFP.

Normalization is found to generate synergistic results when used with combination therapy. This synergy may be coming from the decrease in hypoxia which makes tumor cells more sensitive to both chemotherapy and radiotherapy [25, 26]. Another contribution of this synergy may be its potential benefit in drug delivery.

In addition to that some antiangiogenic agents exhibit proangiogenic effects promoting angiogenesis when they are used in low doses [27, 28]. Increasing vessel density and leakiness proangiogenesis are shown to increase oxygenation and help the delivery of the drugs [29]. Figure 2.7 summarizes three different strategies for manipulating tumor vasculature [30]. Destruction of vessels occurs when there is an excess of antiangiogenic agents in the tumor microenvironment. When antiangiogenic agents are given in an amount to balance the proangiogenic agents, vessel normalization appears. External application of proangiogenic drugs further increases the vessel density.

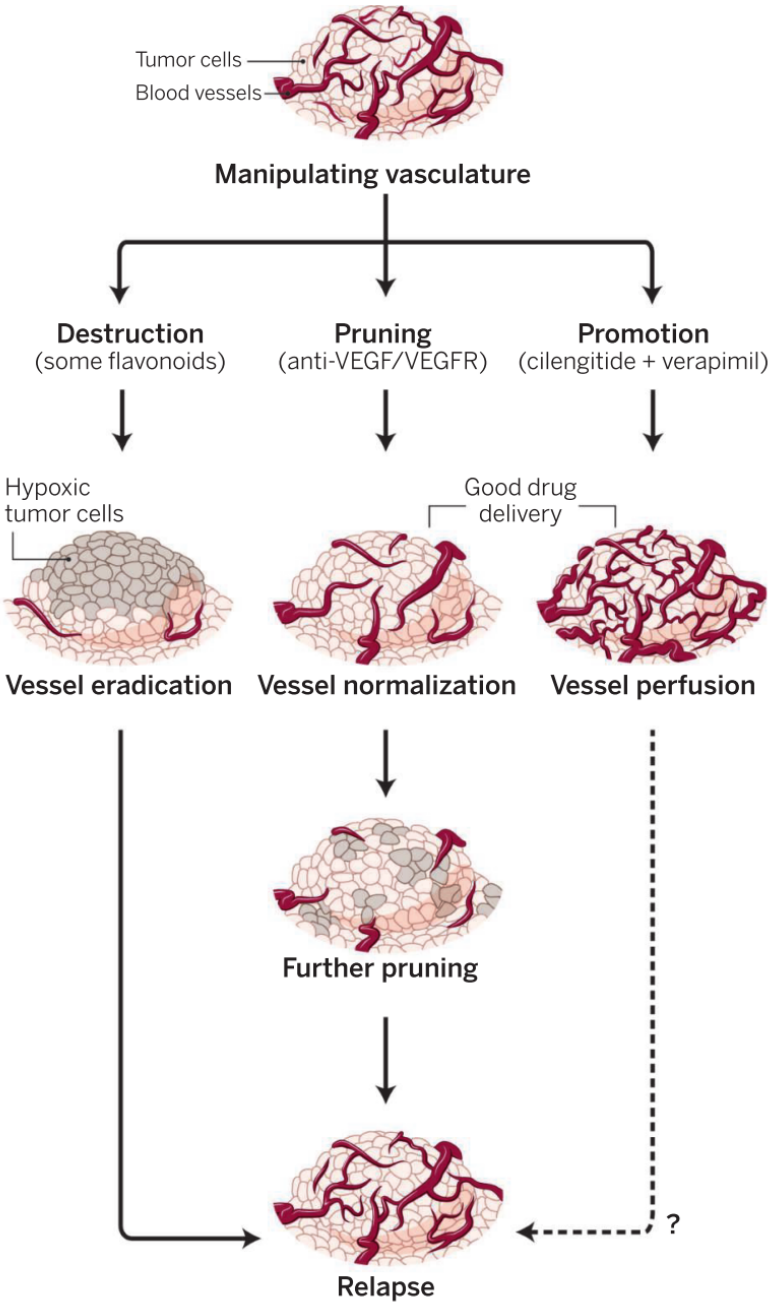

Figure 2.7. Effects of therapies manipulating tumor vessels [30].

2.5. Drug Delivery in Tumors

Due to heterogeneity in the tumor microenvironment, sending drugs to tumor cells are more problematic compared to healthy tissue. The primary source of heterogeneity is abnormal tumor vessels. Vessels produced by angiogenesis mostly reside on tumor peripheral region [15]. Due to solid and fluid pressures, vessels in the interior region of tumors begin to collapse [20]. In addition to that, some of these vessels do not have blood flow due to their tortuosity [9,31]. Because of this heterogeneity in vessels, some parts of tumor do not have access to blood perfusion which would carry the drugs to tumor cells.

Fluid pressure in vessels should be higher than the fluid pressure in tissue (IFP) to maintain fluid extravasation from vessels to tissue. Fluid comes out from vessels at a rate proportional to this difference [32]. The excess fluid in tissue is then collected by the lymph system in healthy tissue at a rate proportional to IFP since the fluid pressure inside lymph vessels are approximately zero [33]. Extravasated fluid in the tissue, interstitial fluid (IF), then move along the IFP gradients in tissue. Due to the increased leakiness as a result of angiogenesis, fluid starts to come out at a higher rate in tumors than in healthy tissue. This fluid begins to accumulate in the tumor. Lymph vessel also being collapsed from solid and fluid pressure and unfunctional enhances this fluid accumulation and resulting in IFP to build up inside the tumors.

Leakiness of tumor vessels and lack of lymphatic system provide an opportunity for delivering large drugs to the tumor called enhanced permeability and retention effect (EPR) [9]. Large drugs which are extravasated exclusively from tumor vessels having large pores in the body starts to accumulate around tumor vessels and stay there long times to act on tumor cells due to lack of collection from lymph system.

On the other hand, severe IFP increase in tumors diminishes the difference between MVP and IFP, inhibiting any fluid extravasation by convection especially in the central regions of the tumor.

Commonly observed IFP profile with a plateau of high IFP in the tumor center and sharply reducing to normal tissue pressure levels at tumor boundary, causes abnormal fluid movements [19, 34]. In the plateau region of IFP, no fluid movement occurs since there is no fluid pressure gradient in that region. Delivery of drugs that depend on convective transport fails when the fluid flow is not present. In the tumor boundary where there is a significant pressure gradient, fluid moves from tumor to normal tissue sweeping the drugs with that flow.

High IFP can also affect blood perfusion inside the vessels. If IFP increases up to MVP around the vessels having large pores, the pressure gradient responsible for the blood flow inside the vessels diminishes creating flow stasis [35, 36]. A vessel in that state can no longer supply the tumor with drugs.

Drugs that are carried by blood flow pass to tumor tissue by convective and diffusive transport from blood vessels. After they extravasated, drugs continue to move along the tissue due to diffusive and convective transport. According to the size of the drug, the main transport mechanism differs. While the delivery of small drugs depends on diffusion, large drugs depend on convection. The main mode of transport can be determined by calculating the Peclet number. The path of drugs is depicted in Figure 2.8.

High IFP creates a barrier for the delivery of large drugs by inhibiting convection from the vessels and in the tumor tissue. Therefore, large drugs can extravasate only in the peripheral region of tumors where later they are swept away towards healthy tissue by the fluid flow. This state of delivery is worsened by the lack of functional vessels in the central region of the tumor, overall resulting heterogeneous drug distribution by inefficient delivery of large drugs in central regions of the tumor. Delivery of small drugs depends on the availability of functional vessels inside the tumor. Due to the heterogeneity of the tumor vasculature, small drugs also delivered to peripheral regions of the tumor.

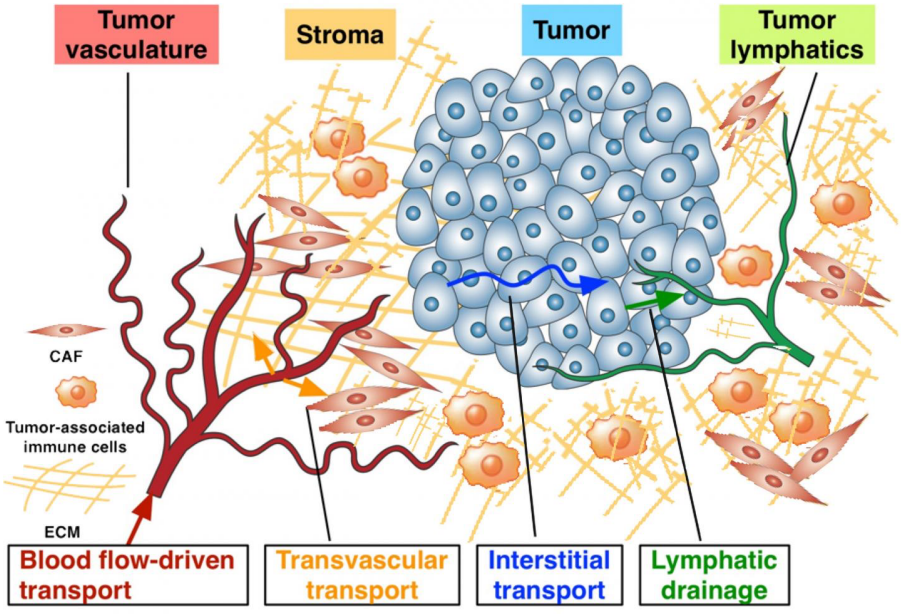

Figure 2.8. Transport in tumor microenvironment [37].

Diffusion and convection of small and large drugs inside the tumor tissue also affected by structure and density of ECM. ECM remodeled by tumor is usually denser creating a barrier for delivery. In some tumors, the desmoplastic reaction occurs by building a dense ECM capsule around tumor blocking the drug delivery which is associated with chemoresistance [38].

3. DEVELOPEMENT OF TUMOR GROWTH AND TREATMENT RESPONSE MODEL

We developed a mathematical model to simulate tumor to observe the interaction between tumor and its microenvironment and to quantify the response to various combination therapies. Two-dimensional model includes tumor cell density, vessel density, IFP and densities of various drugs and their nonlinear interactions. Tumor vessels designed to replicate the heterogeneity, and common patterns in real tumors. Vessels act as a distributor of fluid and various drugs to tumor according to physical transport laws.

3.1. Tumor Growth

Tumor growth dynamics varies between different kind of tumors and even among tumors of the same type. Tumor growth can be modeled using discrete and continuous approaches. Discrete models approach tumor growth by considering a tumor mass consist of discrete cells [39, 40]. Each cell divides and interacts with its microenvironment. Due to the massive number of cells in tumors (10^9 cells in $1cm^3$ of tumor [41]), this approach is used to simulate very small cell populations limited by computational power.

For continuous models, ecological models adapted to represent tumor cell population growth. Tumor growth dynamics are fitted to exponential, surface, sigmoid, atypical, and multistep growth models [42]. Exponential growth better fits growth dynamics of certain non-solid tumors. Surface growth assumes that tumor grows only from a thin layer of dividing cells in the surface. Sigmoid growth models which are a family of models with various types are the most commonly used approach to represent tumor growth consisting of initial exponential phase linear phase followed by a plateau. Atypical models produce sub-cubic growth for solid tumors and sub-exponential growth for non-solid tumors. Multistep models are designed to account for irregular growth

patterns caused by major events like the acquisition of a new mutation. The governing equations for these models are given in Table 3.1 where p represents tumor cell population, $\kappa, \kappa_1, \kappa_2, a$ and b are model parameters used to fit the experimental data into models.

Table 3.1. Models explaining tumor growth [42].

Model type	**Governing equation**
Exponential growth	$dp/dt = \kappa p$
Surface growth	$dp/dt = \kappa\sqrt{p}$
Sigmoid growth	$dp/dt = \kappa_1 p^a - \kappa_2 p^b$

We chose logistic growth which is a sigmoid type growth equation to replicate the increase in cell density (Equation 3.1 second term in right-hand side). The term enables the tumor to grow up to a limiting capacity n_{lim} determined by microenvironmental conditions. In continuous spatial growth models, tumor growth term is accompanied by a term representing the dispersion of tumor cells around the computational domain. In our framework, we utilize a diffusion term for that reason (Equation 3.1 the first term in the right-hand side). Tumor growth coupled the vessel density to account for enhanced growth with the availability of nutrients provided by blood vessels (Equation 3.1 the last term in right-hand side). Hence, the evolution of tumor cell density in the computational domain can be calculated by Equation 3.1,

$$\frac{\partial n(\mathbf{x},t)}{\partial t} = D_n \nabla^2 n(\mathbf{x},t) + rn\Big(1 - \frac{n}{n_{lim}}\Big) + \alpha_{mn} n(\mathbf{x},t) m(\mathbf{x},t) \tag{3.1}$$

where $n(\mathbf{x},t)$ is tumor cell density, D_n is diffusion coefficient for tumor cells, r is the growth rate, n_{lim} is the carrying capacity, α_{mn} is the coupling coefficient to vessels.

Additional terms can be added to Equation 3.1 to simulate effect of various drugs. Effect of cytotoxic and cytostatic drugs may be included according to their Pharmacodynamic (PD) relations with the tumor.

Drug activity is measured by measuring plasma drug concentration and tumor response to therapy. It varies from log-linear dose–response to responses that plateau after relatively small concentration increments [5]. The activity of cytotoxic drugs on tumor cells may be added with a minus term to Equation 3.1 that include the reaction of tumor cells with drug concentration for various reaction type. Cytostatic drugs may be added manipulation of tumor growth terms accordingly. Examples of both can be found in Chapters 4 and 5. The simulations for tumor cell density demonstrates tumor growth in Figure 3.1.

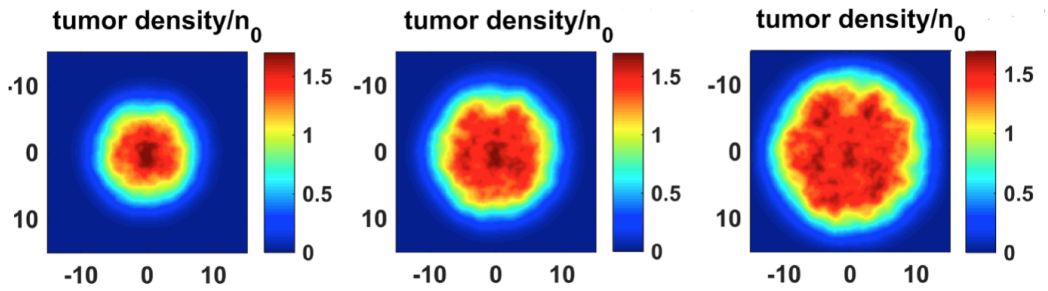

Figure 3.1. Tumor growth in simulations.

3.2. Vessel Growth

In mathematical models, vessel structure can be chosen to be continuous or discrete according to according to the scope of the model. Discrete vessels provide the convenience to include intravascular flow dynamics. They can be used to calculate blood flow along the vessels by Poiseulle's law for ideal pipe flow [43],

$$Q = -\frac{\pi\rho^4}{128\eta}\frac{dP_v}{dx} \tag{3.2}$$

where Q axial flow, ρ is vessel diameter, η is blood viscosity, and P_v is vascular pressure.

In this model, we used the heterogeneous vessel structure proposed by Kohandel *et al.* [44],

$$\frac{\partial m(\mathbf{x},t)}{\partial t} = D_m \nabla^2 m(\mathbf{x},t) + m(\mathbf{x},t)\big(\alpha + \beta m(\mathbf{x},t) + \gamma m(\mathbf{x},t)^2\big) \tag{3.3}$$

where $m(\mathbf{x},t)$ is the density of tumor vessels, D_m is the diffusion coefficient for vessels, α, β and γ are phenomenological parameters for vessel growth. Local vessel growth is represented in the second term in right-hand side, and the distribution of vessels are represented by diffusion in the first term in the right-hand side of Equation 3.3. Equation have two stable points at $m = 0$ and $m = 1$ and one unstable point in $m = 1/2$ creating vessel islands.

Additional terms for angiogenic vessel growth may be added to Equation 3.3 according to the scope of the model. Two different angiogenesis models are included in Chapters 4 and 5. The simulations for tumor vessel density demonstrates vessel growth in Figure 3.2.

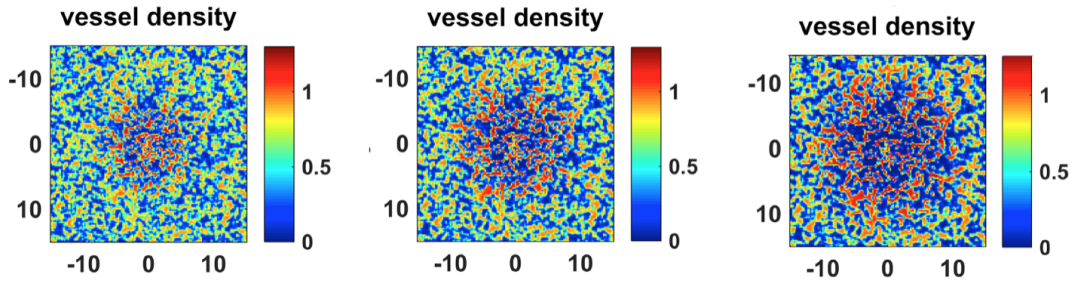

Figure 3.2. Vessel growth in simulations.

3.3. Interstitial Fluid Pressure

In the lenght scale we build our model (order of $10^{-1}mm$), interstitial fluid can be approximated to be continuous [45]. For a small element of volume V which has a surface S, the mass is equal to $\int_V \rho dV$ where ρ is the density of fluid element. Then the decrease in mass of a fluid element of volume V is given by

$$-\frac{d}{dt}\int_V \rho dV = -\int_V \frac{d\rho}{dt} dV. \tag{3.4}$$

To conserve the mass, this quantity should be equal to fluid flux coming out from the surface S of the volume element,

$$-\int_V \frac{d\rho}{dt} dV = \int_S \rho \mathbf{u} dS. \tag{3.5}$$

By the divergence theorem Equation 3.5 is equal to,

$$\int_S \rho \mathbf{u} dS = \int_V \boldsymbol{\nabla}.(\rho \mathbf{u}) dV. \tag{3.6}$$

Hence mass conservation for unit volume V becomes,

$$\int_V \frac{d\rho}{dt} dV + \int_V \boldsymbol{\nabla}.(\rho \mathbf{u}) dV = 0. \tag{3.7}$$

Since this equation should hold over the whole volume, continuity condition becomes,

$$\frac{d\rho}{dt} + \boldsymbol{\nabla}.(\rho \mathbf{u}) = 0. \tag{3.8}$$

which can be expanded into,

$$\frac{d\rho}{dt} + \mathbf{u}\boldsymbol{\nabla}\rho + \rho\boldsymbol{\nabla}.\mathbf{u} = 0. \tag{3.9}$$

The first two terms in the left-hand side of Equation 3.9 is equal to the material derivative $D\rho/Dt$. Hence the equation becomes,

$$\frac{D\rho}{Dt} + \rho \boldsymbol{\nabla}.\mathbf{u} = 0. \tag{3.10}$$

If the fluid is incompressible, in another words, ρ is constant, $D\rho/Dt = 0$. Then we have the relation for mass continuity as,

$$\boldsymbol{\nabla} \cdot \mathbf{u} = 0. \tag{3.11}$$

This is the condition for flow inside the tumor tissue when there is no sources and sinks are available. In this framework, we have heterogeneously distributed fluid sources inside the tissue which are the tumor blood vessels and sinks which are the lymph vessels. Interstitial fluid builds up inside tumor tissue by the interchange fluid from these sources and sinks into the tumor. For the steady-state fluid flow, the continuity equation inside the tumor is:

$$\boldsymbol{\nabla} \cdot \mathbf{u} = J_{fluid}, \tag{3.12}$$

$$J_{fluid} = \Gamma_b - \Gamma_\ell, \tag{3.13}$$

where J_{fluid} is the net fluid flux, Γ_b (1/s) represents the supply of the fluid from blood vessels into the interstitial space and Γ_ℓ (1/s) represents the fluid drainage from the interstitial space into the lymph vessels.

Starling equation determines the fluid flux from vessels by taking into account hydrostatic and oncotic forces.

$$\Gamma_b = \lambda_b m(\mathbf{x}, t)[P_v - P(\mathbf{x}, t) - \sigma_v(\pi_c - \pi_i)], \tag{3.14}$$

The same relation can be used to calculate the fluid flux from tissue to lymph vessels. Assuming that the pressure inside the lymph vessels are approximately zero [33] and the osmotic pressure contribution for the lymph vessels is negligible due to the highly permeable lymphatics, lymph collection is equal to:

$$\Gamma_\ell = \lambda_\ell P(\mathbf{x}, t). \tag{3.15}$$

Hence the continuity equation becomes:

$$\boldsymbol{\nabla} \cdot \mathbf{u} = \Gamma_b - \Gamma_\ell, \tag{3.16}$$

$$\boldsymbol{\nabla} \cdot \mathbf{u} = \lambda_b m(\mathbf{x}, t)[P_v - P(\mathbf{x}, t) - \sigma_v(\pi_c - \pi_i)] - \lambda_\ell P(\mathbf{x}, t). \tag{3.17}$$

The parameters in these equations are the hydraulic conductivities of blood vessels λ_b and the lymphatics λ_ℓ, the vascular pressure P_v, interstitial fluid pressure P and the osmotic reflection coefficient σ_v. The capillary and the interstitial oncotic pressures are denoted by π_c and π_i, respectively. Hydraulic conductivities of blood and lymph vessels are related to the hydraulic conductivity of vessel wall (L_p) and the vessel surface density ($\frac{S}{V}$) with the relation $\lambda_{b,\ell} = L_p \frac{S}{V}$.

Darcy's law is decribes the flow through porous medium. Here, we use it to describe the interstitial fluid flow within the tissue:

$$\mathbf{u} = -K \boldsymbol{\nabla} P, \tag{3.18}$$

where K is the hydraulic conductivity of the interstitium (mm^2/s/mmHg) and P is the interstitial fluid pressure (IFP). By substituting Darcy's law into continuity equation, we obtain the expression:

$$\boldsymbol{\nabla} \cdot \mathbf{u} = -\boldsymbol{\nabla} \cdot (K \boldsymbol{\nabla} P) \tag{3.19}$$

Assuming that K is uniform through the tissue,

$$\boldsymbol{\nabla} \cdot \mathbf{u} = -K \nabla^2 P \tag{3.20}$$

By substituting Starling's law into the continuity equation, we obtain the equation for IFP in a solid tumor:

$$-K \nabla^2 P(\mathbf{x}, t) = \lambda_b m(\mathbf{x}, t) \left[P_v - P(\mathbf{x}, t) - \sigma_v (\pi_c - \pi_i) \right] - \lambda_\ell P(\mathbf{x}, t). \tag{3.21}$$

3.4. Generalized Drug Equation

Pharmacokinetic (PK) models can be used to calculate the drug concentration in the tumor site [46]. Physiology-based pharmacokinetic models are built which are composed of compartment models to track how much drug reaches the tumor [47]. Compartment models divide the biological system to its parts to calculate how drugs reach the intended sites. Each part is represented by a compartment which is a uniform entity without spatial variation. For each compartment, there are rules for physical transportation, absorption, metabolism, and elimination. Ordinary differential equations (ODEs) are used to build the compartment models. This model type calculates steady-state distributions of drugs; therefore it lacks explaining the time-dependent effects of the drugs [47].

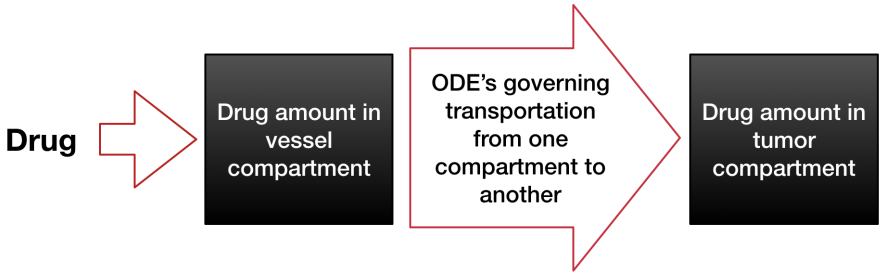

Figure 3.3. A simple compartment PK model for drug delivery in the tumor.

The effect of the drug on the target site is the subject of pharmacodynamic (PD) models. Activation, reaction and binding relations of the drugs are quantified for each compartment when they are applicable. Mechanistic drug interactions build by the receptor theory [47]. Dynamical system analysis is used to explore the PK/PD systems. PK/PD models together provide the information to optimize the planning of dose and schedule of the drug. Combination of PK and PD results are demonstrated in Figure 3.4.

Even though PK/PD models are crucial for understanding dose and response relationships, the adaptation of them to tumors may not be reliable due to the tumors being spatially heterogeneous. When the drugs do not reach to certain parts of tumor in effective doses due to the barriers mentioned in this thesis, tumors may develop drug resistance. Hence, it may be more suitable to couple PK/PD models to a spatiotemporal modeling framework [49].

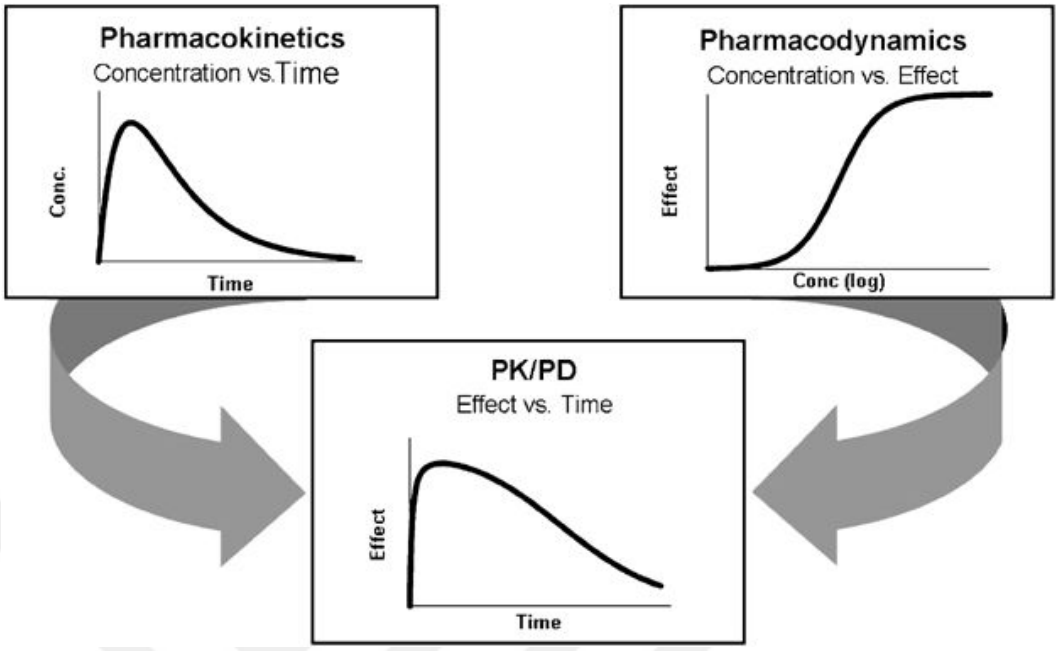

Figure 3.4. PK/PD models to analyze drug delivery and response [48].

In this framework, to simulate drug delivery and activity, we tried to combine PK/PD relations with our spatiotemporal tumor growth model. Drugs are carried to the tumor by blood vessels and distributed through tumor microenvironment via diffusion and convection. Vessels behave as spatially heterogeneous sources of the drugs. Drugs that reach the tumor microenvironment act on their targets.

To quantify the drug distribution, a generalized equation is formed to account for all paths of delivery, Equation 3.22:

$$\frac{\partial d_i(\mathbf{x},t)}{\partial t} = D_i\nabla^2 d_i(\mathbf{x},t) + \nabla\cdot(k_E d_i(\mathbf{x},t)K\nabla P) + \lambda_i m(\mathbf{x},t)\big(d_v^i - d_i(\mathbf{x},t)\big) + \Gamma_b(1-\sigma_i)d_v^i - \Gamma_\ell d_i(\mathbf{x},t) - k_i d_i(\mathbf{x},t), \quad (3.22)$$

where $d_i(\mathbf{x},t)$ is the concentration of drug of choice, D_i is the diffusion coefficient in tumor tissue, k_E is the retardation coefficient for interstitial convection, λ_i is the transvascular diffusion coefficient of the drug, d_v^i is the plasma drug concentration, σ_i is the solvent drag reflection coefficient, and k_i is the decay rate of the drugs. Drug

extravasate from vessels by diffusion and convection in third and fourth terms in the right-hand side of Equation 3.22, respectively. Then, they diffuse and convect through tumor tissue in the first and second terms on the right-hand side. The fifth term is the lymphatic collection, and the last term is the natural decay of the drug. Diffusion or convection terms can be eliminated according to the main mode of transportation of the drug determined by its size and microenvironmental properties.

Decrease in the drug amount in tumor microenvironment due to the activity the drugs on tumor cells and vessels may be added to the Equation 3.22 with a minus term according to their PD relations.

3.5. Solution Method

Complete models including interaction terms between components are constructed in Chapters 4 and 5 on this base framework. In complete models, we have various coupled nonlinear PDEs that have to be calculated simultaneously. We employed the finite difference method for numerical solution of the equation system. Equations converted into their dimensionless forms before construction of iterative solution scheme.

The idea behind the finite difference method comes from the definition of derivative of a smooth function $u(x)$,

$$u'(x) = \lim_{h \to 0} \frac{u(x+h) - u(x)}{h}. \tag{3.23}$$

If we discretize our spatiotemporal domain in small enough pieces, we can approximate the solution of our PDEs iteratively in for all space and time points through simulations. The finite difference method for calculation of derivatives comes from the Taylor expansions of that function which are given in Equations 3.24 and 3.25 [50]:

$$u(x+h) = u(x) + hu'(x) + \frac{h}{2}u''(x) + \frac{h}{6}u^{(3)}(x) + \frac{h}{24}u^{(4)}(\xi^{+}) \tag{3.24}$$

$$u(x-h) = u(x) - hu'(x) + \frac{h}{2}u''(x) - \frac{h}{6}u^{(3)}(x) + \frac{h}{24}u^{(4)}(\xi^-) \tag{3.25}$$

where $\xi^+ \in]x, x+h[$ and $\xi^- \in]x-h, x[$. If we subtract the Equation 3.25 from the Equation 3.24, we reach the expression for the first derivatives:

$$u'(x) + \frac{h^2}{6}u^{(3)}(\xi) = \frac{u(x+h) - u(x-h)}{2h}. \tag{3.26}$$

Hence, the central difference method is given by Equation 3.27, which ensures that for small h:

$$u'(x) = \frac{u(x+h) - u(x-h)}{2h} \tag{3.27}$$

with error $|\frac{h^2}{6}u^{(3)}(\xi)| \leq Ch^2$, where $C = \sup_{y\in[x-h_0,x+h_0]} \frac{|u^{(3)(y)}|}{6}$ with $\xi \in]x-h, x+h[$ and $h \in]0, h_0[$.

Second derivatives can be found adding Taylor expansions, Equations 3.24 and 3.25,

$$u''(x) + \frac{h^2}{12}u^{(4)}(\xi) = \frac{u(x+h) - 2u(x) + u(x-h)}{h^2} \tag{3.28}$$

with error $|\frac{h^2}{12}u^{(4)}(\xi)| \leq Ch^2$, where $C = \sup_{y\in[x-h_0,x+h_0]} \frac{|u^{(4)(y)}|}{12}$ with $\xi \in]x-h, x+h[$ and $h \in]0, h_0[$. Hence, the central difference method is given by Equation 3.29, which ensures that for small h:

$$u''(x) = \frac{u(x+h) - 2u(x) + u(x-h)}{h^2} \tag{3.29}$$

To find numerical solutions, we created a grid to solve the discretized versions of dimensionless model equations according to the finite difference method. The 2-D grid is composed of $151x151$ space grid points divided by uniform steps of dx and dy where $dx = dy = 0.063mm$ given in Figure 3.5. Numerical solutions of PDEs are found for

each space grid point in between time intervals divided to 1401 uniform steps of time length dt where $dt = 0.52 hours$.

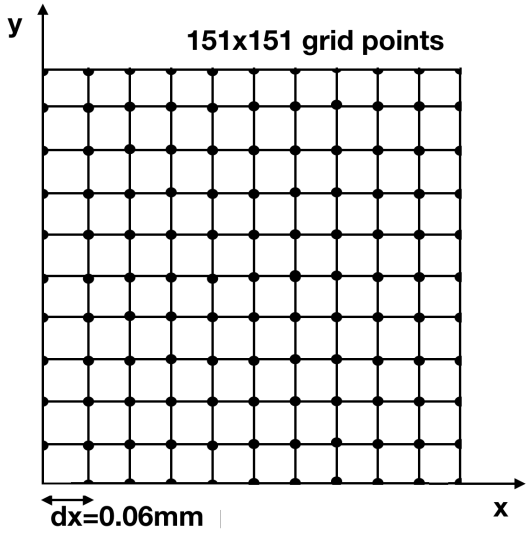

Figure 3.5. Spatial computational domain.

In 2-D space grid, the finite difference method for derivatives can be written as:

$$u'_{i,j} = \frac{u_{i+1,j} - u_{i-1,j}}{2dx} \tag{3.30}$$

for the first derivatives in x, and for second derivatives in x, it is equal to:

$$u''_{i,j} = \frac{u_{i+1,j} - 2u_{i,j} + u_{i-1,j}}{dx^2} \tag{3.31}$$

After implementing discretization of space and time in difference equations, initial values are given as input to calculate updated values of derivatives in each space point in each time iteration. On the boundaries, specific boundary conditions are used for each biologic components which can be found in detail in Chapter 4 and 5.

Model is composed of equations with different characteristic times. Tumor and vessel growth (slow equations) have a much longer characteristic time compared to that of change in pressure and dispersion of chemicals (fast equations) in the computational domain. We discretize dx, dy, and dt to values associated with tumor and vessel growth. Therefore, all fast equations are solved in steady-state.

Jacobi method is used to calculate the convergent values of steady-state solutions for each time step. First, these steady state equations are discretized by the finite difference method in space. Initial values $u^0(\mathbf{x})$ are given as input, and pseudo-time stepping progress is applied to find the updated values. The solutions in whole spatial domain are updated until difference of two adjacent solution in pseudo time is approximately zero ($u^{n+1}(\mathbf{x}) - u^n(\mathbf{x}) \approx 0$). This is the convergence condition, and when it is reached, the pseudo-time iteration stops, giving the steady-state solution for each fast equation between each time step dt.

Steady-state equations are discretized in space since they have no time dependency at a specific time step. All of our steady-state equations of the form given in Equation 3.32 having a Laplacian:

$$\nabla^2 u(x, y) = f(u(x, y)), \tag{3.32}$$

which can be expanded as:

$$\frac{\partial^2 u(x, y)}{\partial x^2} + \frac{\partial^2 u(x, y)}{\partial y^2} = f(u(x, y)), \tag{3.33}$$

We discretize the equation using finite difference method, we acquire the equation:

$$\frac{u_{i+1,j} - 2u_{i,j} + u_{i-1,j}}{dx^2} + \frac{u_{i,j+1} - 2u_{i,j} + u_{i,j-1}}{dy^2} = f(u_{i,j}), \tag{3.34}$$

since dx and dy is equal, we can rewrite the Equation 3.34 as,

$$u_{i,j} = \frac{1}{4}(u_{i+1,j} + u_{i-1,j} + u_{i,j+1} + u_{i,j-1}) - \frac{1}{4}f(u_{i,j})dx^2. \tag{3.35}$$

Then using Jacobi method, we introduce the pseudo-time progression to find subsequent values:

$$u_{i,j}^{n+1} = u_{i,j}^{n} + \frac{1}{4}(u_{i+1,j}^{n} + u_{i-1,j}^{n} + u_{i,j+1}^{n} + u_{i,j-1}^{n} - 4u_{i,j}^{n}) - \frac{1}{4}f(u_{i,j}^{n})dx^2. \tag{3.36}$$

This equation can be divided to two parts:

$$u_{i,j}^{n+1} = u_{i,j}^{n} + \Delta u_{i,j}^{n}. \tag{3.37}$$

The first term in right-hand side $u_{i,j}^{n}$ which is the value from the previous iteration and the second term $\Delta u_{i,j}^{n}$ which is the residual part of the nth iteration. After many iterations, the residual part should become smaller approaching to zero and finally converge into the steady-state value of the equation. Once, steady state values of fast equations are found for time step k, time dependent slow equations are calculated taking into account their interactions with solutions of fast equations.

4. EFFECT OF NORMALIZATION IN CHEMOTHERAPY DELIVERY AND RESPONSE

The abnormal structure of tumor vasculature is one of the leading causes of insufficient and spatially heterogeneous drug delivery in solid tumors. Tortuous and highly permeable tumor vessels along with the lack of a functional lymphatic system cause interstitial fluid pressure (IFP) to increase within tumors. This elevated IFP results in the inefficient penetration of large drug particles into the tumor, whose primary transport mechanism is convection [19, 51].

The abnormalities in tumor vasculature are caused by dysregulation of angiogenesis. Tumors initiate angiogenesis to form a vascular network that can provide oxygen and nutrients to sustain its rapid growth. The production of VEGF, a growth factor that promotes angiogenesis, is triggered by the chronic hypoxic conditions that are prevalent in tumors. Besides inducing angiogenesis, it leads to hyperpermeable blood vessels by enlarging pores and loosening the junctions between the endothelial cells that line the capillary wall [3, 52]. Subsequently, excessive fluid extravasation from these vessels results in a uniformly elevated IFP in the central region of tumor nearly reaching the levels of microvascular pressure (MVP) while at the tumor periphery, IFP falls to normal tissue levels [51, 53, 54]. This common profile of IFP within tumors has been identified as a significant transport barrier to therapeutic agents and large molecules [51, 55]. When IFP approaches MVP, pressure gradients along vessels are diminished and blood flow stasis occurs, diminishing the functionality of existing vessels [36, 56, 57]. Furthermore, uniformity of IFP in interior regions of tumors terminates the convection within tumor interstitium, hindering the transportation of large drugs [51]. While the lack of a transvascular pressure gradient inhibits convective extravasation of drugs, sharp IFP gradient at tumor periphery creates an outward fluid flow from tumors that sweeps drugs away into normal tissues [51]. Together these factors lead to the decreased drug exposure of tumor cells.

It has been revealed that the application of antiangiogenic agents can decrease vessel wall permeability and vessel density, transiently restoring some of the normal function and structure of abnormal tumor vessels [2,3,58]. This process, which is called vascular normalization, is associated with a decrease in IFP and an increase in perfusion. Therefore, this state of vasculature enables increased delivery of both drug and oxygen/nutrients to the targeted tumor cells [58, 59]. Normalization enhances convection of drug particles from vessels into tumor interstitium by restoring transvascular pressure gradients through IFP reduction [32, 35, 58]. It has shown some favorable results in preclinical and clinical trials regarding the enhancement of the delivery of large therapeutics such as nanoparticles [35, 60, 61]. Since nanoparticles benefit from the enhanced permeability and retention effect (EPR), they are distributed in higher amounts to tumors relative to normal tissue. Accumulation of nanoparticles in normal tissues is relatively small compared to the standard small molecule chemotherapies, leading to decreased toxicity and side effects. However, the main transport mechanism for large drugs is convection in tumor microenvironment. Hence, when IFP is high, extravasation via convection is inhibited. Normalization due to its ability to decrease IFP seems promising in drug delivery for large drugs with its potential of restoring convective transportation.

In both clinical and preclinical studies, it has been shown that antiangiogenic drugs demonstrate anti-tumor effects in various cancer types [62]. However, rather than using antiangiogenic agents alone, studies reveal that the combination of these agents with chemotherapy drugs yields favorable results with increased therapeutic activity. In some clinical studies [63–65], bevacizumab combined with conventional chemotherapy has increased the survival and response rates among patients with gastrointestinal cancer compared to bevacizumab alone. This finding that antiangiogenic therapy in combination with chemotherapy can improve the efficacy of treatment has been observed for patients with various cancers including non-small cell lung cancer [66, 67], breast cancer [68–70] and ovarian cancer [71].

It is evident that there is a transient time window for vessel normalization [72,73]. In order to improve drug delivery, chemotherapy should coincide with this transient state of improved vessel integrity. Prolonged or excessive application of antiangiogenic agents can reduce microvascular density to the point that drug delivery is compromised [74]. Therefore, dosing and scheduling of combined therapy with antiangiogenic agents must be carefully tailored to augment the delivery and response to chemotherapy [2]. It is suggested that rather than uninterrupted application, intermittent cycles which can create re-normalization should be employed for antiangiogenic agent scheduling [75].

4.1. Related Literature Review in Modeling of Tumor

Due to the complex and interdisciplinary nature of the subject, there is a considerable amount of computational efforts on tumor vascularization and its consequences for the tumor microenvironment and drug delivery. Development of vasculature and intravascular flow dynamics are studied comprehensively [18, 20, 76–79] and in many studies chemotherapy is given through the discrete vessel system in order to calculate drug delivery to capillaries and tumor [20, 76, 77, 79, 80]. Mathematical models have included transvascular and interstitial delivery of drugs [20, 79, 80]. In addition to that, Wu *et al.* added tumor response to chemotherapy by applying nanoparticles and evaluating the decrease in tumor radius during chemotherapy for different microenvironmental conditions [20]. There are also some studies about the optimization of combination therapy in tumors [81]. In studies by the groups of Urszula Ledzewicz and Heinz Schäettler, changes in tumor volume after the administration of cytotoxic and antiangiogenic agents have been investigated by proposing a mathematical model and seeking optimal solutions for different treatment cases [82,83]. Compartment models have also been used to explore how antiangiogenic agents may provide assistance to chemotherapy agents in reducing the volume of drug-resistant tumors, and by using a bifurcation diagram it is shown that the co-administration of antiangiogenic and chemotherapy drugs can reduce tumor size more effectively compared to chemotherapy alone [84].

Applications of chemotherapy drugs together with antiangiogenic agents have been studied by Panovska *et al.* to cut the supply of nutrients [85]. Stephanou *et al.* showed that random pruning of vessels by anti-angogenic agents improves drug delivery by using 2-D and 3-D vessel networks [86]. However, they did not associate this benefit with normalization of vasculature. Jain and colleagues laid out the general groundwork for relations between vessel normalization and IFP by relating vessel properties and interstitial hydraulic conductivity to changes in pressure profile due to normalization [32]. The subject is further investigated by Wu *et al.* by building a 3-D model of angiogenesis and adding intravascular flow to the computational framework [18]. They observed slow blood flow within the tumors due to almost constant MVP and elevated IFP profile. They show the coupling between intravascular and transvascular flux. Kohandel *et al.* showed that normalization enhances tumor response to chemotherapy and identified the most beneficial scheduling for combined therapy in terms of tumor response [44]. The size range of nanoparticles that could benefit from normalization has also been investigated [60].

4.2. Mathematical Model

In this study, following the continuous mathematical model developed by Kohandel *et al.* [44] which couples tumor growth and vasculature, we built a framework for tumor dynamics and its microenvironment including IFP. We use this system to evaluate the improvement in nanoparticle delivery resulting from vessel normalization. As the tumor grows, a homogeneous distribution of vessels is altered by the addition of new leaky vessels to the system, representing angiogenesis. As a consequence of angiogenesis and the absence of lymph vessels, IFP starts to build up inside the tumor inhibiting the fluid exchange between vessels and tumor and inhibiting nanoparticle delivery. Simulations give the distribution of the nanoparticles in the tumor in a time-dependent manner as they exit the vessels and are transported through interstitium. The activity of the drugs on tumor cells is determined according to the results of experimental trials by Sengupta *et al.* [87]. We apply drugs in small doses given in subsequent bolus injections. During drug therapy, both vessels and tumor respond

dynamically. After injections of antiangiogenic agents, a decrease in vessel density accompanies the changes in vessel transport parameters, initiating the normalized state. Combining chemotherapy with applications of antiangiogenic agents, we are able to identify the benefits of a normalized state by observing the effects of different scheduling on IFP decrease, extravasation of drugs and tumor shrinkage. We found that in adjuvant combination of drugs, IFP and vessel density decrease together resulting in an increase in the average extravasation of nanoparticles per unit area in the interior region of tumor. In concurrent combination of drugs, IFP decrease is higher but vessel decrease is higher as well, creating a smaller enhancement in average extravasation per unit tumor area. However, even though average extravasation is smaller in this case, we observe an increase in homogeneity in drug distribution. Nanoparticles begin to extravasate even in the center of tumor through sparsely distributed vessels due to the sharp decrease in IFP. Therefore normalization enabled the drugs to reach deeper regions of the tumor.

4.3. Model Equations

4.3.1. Tumor cells, vasculature and IFP

Following Kohandel *et al.* [44], the Equations 4.1 and 4.2 are used to model the spatio-temporal distribution of tumor cells and the heterogeneous tumor vasculature. In Equation 4.1, the first term models the diffusion of tumor cells, where D_n is the diffusion coefficient, and the second term describes the tumor growth rate, where n_{lim} is the carrying capacity and r is the growth rate. In the absence of the third and fourth terms, the Equation 4.1 has two fixed points: an unstable fixed point at $n = 0$ where there is no cell population and a stable fixed point at $n = n_{lim}$ where the population reaches its maximal density. The coupling terms $\alpha_{mn} n(\mathbf{x}, t) m(\mathbf{x}, t)$ and $d_r n(\mathbf{x}, t) d(\mathbf{x}, t)$ indicate the interactions of tumor cells with vasculature and chemotherapy drug, respectively. Tumor cells proliferate at an increased rate α_{mn} when they have vessels supplying them with nutrients and tumor cells are eliminated at rate d_n if chemotherapy drug $d(\mathbf{x}, t)$

is present.

$$\frac{\partial n(\mathbf{x},t)}{\partial t} = D_n \nabla^2 n(\mathbf{x},t) + rn\Big(1 - \frac{n}{n_{lim}}\Big) + \alpha_{mn} n(\mathbf{x},t) m(\mathbf{x},t) - d_n n(\mathbf{x},t) d(\mathbf{x},t). \quad (4.1)$$

The tumor vasculature network exhibits abnormal dynamics with tortuous and highly permeable vessels which are structurally and functionally different from normal vasculature. In order to create this heterogeneous structure, a coarse-grained model is used to produce islands of vessels. In Equation 4.2, the average blood vessel distribution is represented with m($\mathbf{x}$,t) and the equation is formulated to produce islands of vascularized space with the term $m(\mathbf{x},t)(\alpha + \beta m(\mathbf{x},t) + \gamma m(\mathbf{x},t)^2)$ which has two stable points $m = 1$ and $m = 0$ corresponding to the presence and absence of vessels, respectively. Representation of tumor-induced angiogenesis is modified in this model by recruiting the terms $\alpha_{nm} n(1 - n/n_{lim})m$ and $\beta_{nm} \nabla.(m \nabla n)$. Here, the former attains positive values for tumor periphery due to the low cell density and in the central regions when cell density exceeds n_{lim}, the term becomes negative creating a behavior which resembles to real tumors that has generally high vascularization in periphery and low vessel density in the center due to the growth-induced stresses [88]. The latter term leads the vessels that are produced in the periphery towards the tumor core. In this novel form, parameters relate to angiogenesis, β_{nm} and α_{nm} are changed as 0.5 and 0.25, respectively. Remaining set of the parameters related to tumor and vessel growth can be found in Kohandel *et al.* [44]. $A_r m(\mathbf{x},t) A(\mathbf{x},t)$ is the reaction of tumor vessels to antiangiogenic agent $A(\mathbf{x},t)$, which results in the elimination of vessels in the presence of antiangiogenic agent.

$$\frac{\partial m(\mathbf{x},t)}{\partial t} = D_m \nabla^2 m(\mathbf{x},t) + m(\mathbf{x},t)\big(\alpha + \beta m(\mathbf{x},t) + \gamma m(\mathbf{x},t)^2\big) + \beta_{nm} \nabla \cdot (m \nabla n) + \alpha_{nm} n\Big(1 - \frac{n}{n_{lim}}\Big) m - A_r m(\mathbf{x},t) A(\mathbf{x},t). \quad (4.2)$$

For the initial configuration of tumor cells, a Gaussian distribution is assumed while the initial vascular distribution is obtained by starting from a random, positively distributed initial condition of tumor vessels.

Table 4.1. Interstitial fluid transport parameters.

Parameter	**Unit**	**Tumor**	**Normal**
$[L_P]_{\text{blood}}$	cm/mmHg·s	$1.86\times10^{-6,a}$	$3.6\times10^{-8,a}$
$\left[\frac{S}{V}\right]_{\text{blood}}$	cm^2/cm^3	200^{b}	70^{b}
λ_b	1/mmHg·s	$3.72\times10^{-4,c}$	$2.52\times10^{-6,c}$
λ_ℓ	1/mmHg·s	0^{d}	$6.66\times10^{-4,e}$
P_0	mmHg	15^{a}	15^{a}
$\sigma_v\,(\pi_p - \pi_i)$	mmHg	$2.2\times10^{-4,a}$	9.1^{a}
$P_{\text{eff}}{}^{f}$	mmHg	15	5.9
K	cm^2/mmHg·s	$2.5\times10^{-7,a}$	$2.5\times10^{-7,a}$

[a] [32], [b] [89], [c]calculated from $L_P\frac{S}{V}$, [d] [90, 91], [e] [20] and [f]$P_{\text{eff}} = P_v - \sigma_v\,(\pi_p - \pi_i)$, effective microvascular pressure.

Steady state IFP can be found by substituting Darcy's law and Starling's law into the continuity equation. Detailed derivation can be found on Chapter 3. Interstitial fluid pressure $P(\mathbf{x}, t)$ for each time point is given by the relation:

$$-K\nabla^2 P(\mathbf{x}, t) = \lambda_b m(\mathbf{x}, t)\,[P_v - P(\mathbf{x}, t) - \sigma_v(\pi_c - \pi_i)] - \lambda_\ell P(\mathbf{x}, t). \tag{4.3}$$

Pressure is initially taken to be the normal tissue value P_0 and the initial pressure profile is set based on the solution of the above equation with the initial condition for tumor vasculature. The boundary condition ensures that pressure reduces to the normal value P_0 in host tissue.

4.3.2. Antiangiogenic agent and chemotherapy drug

For the transport of antiangiogenic agents $A(\mathbf{x}, t)$, a diffusion equation is used:

$$\frac{\partial A(\mathbf{x}, t)}{\partial t} = D_A \nabla^2 A(\mathbf{x}, t) + \lambda_A m(\mathbf{x}, t)\big(A_v - A(\mathbf{x}, t)\big) - \Gamma_\ell A(\mathbf{x}, t) - k_A A(\mathbf{x}, t), \quad (4.4)$$

where D_A is the diffusion coefficient of antiangiogenic agents in tissue, λ_A is the transvascular diffusion coefficient of antiangiogenic agents, A_v is the plasma antiangiogenic agent concentration and k_A is the decay rate of antiangiogenic agents. The terms on the right hand side represent the diffusion of the antiangiogenic agents in the interstitium, diffusion through the vessels, the drainage of agents to the lymph vessels and the decay rate of the agents, respectively.

We consider liposomal delivery vehicles for chemotherapy drug with their concentration denoted by $d(\mathbf{x}, t)$. Since they are relatively large ($\sim$ 100 nm), a convection-diffusion equation is used for the transport of these drug molecules:

$$\frac{\partial d(\mathbf{x}, t)}{\partial t} = D_d \nabla^2 d(\mathbf{x}, t) + \nabla \cdot (k_E d(\mathbf{x}, t) K \nabla P) + \Gamma_b (1 - \sigma_d) d_v - \Gamma_\ell d(\mathbf{x}, t) - d_r d(\mathbf{x}, t) n(\mathbf{x}, t) - k_d d(\mathbf{x}, t), \quad (4.5)$$

where D_d is the diffusion coefficient of drugs in the tissue, k_E is the retardation coefficient for interstitial convection, d_v is the plasma drug concentration, σ_d is the solvent drag reflection coefficient, d_r is the rate of drug elimination as a result of reaction with tumor cells and k_d is the decay rate of the drugs. The terms on the right hand side represent the diffusion and the convection of the drugs in the interstitium, convection of the drugs through the vessels, the drainage of the drugs into the lymphatics, the consumption of drugs as a result of tumor cell interaction and the decay of the drug, respectively. Diffusion of the drug from the blood vessels is assumed to be negligible since transvascular transport of large drugs is convection-dominated.

Table 4.2. Parameters related to transport of 100 nm liposomes and antiangiogenic agents.

Parameter	**Unit**	**Tumor**	**Normal**
D_d	cm^2/s	$2.5\times10^{-9,a}$	$2.5\times10^{-9,a}$
k_E	-	0.35^b	0.35^b
$1-\sigma_d$	-	0.87^c	0
P_d	cm/s	$5\%\times3.42\times10^{-7,d}$	$5\%\times0.88\times10^{-7,d}$
λ_d	1/s	$4\times10^{-6,e}$	$1.4\times10^{-7,e}$
λ_r	1/hours	$1/135^f$	$1/135^f$
$t_{1/2}$	hours	45.2^g	45.2^g
d_r	-	1	0
k_d	1/s	1.65×10^{-6}	1.65×10^{-6}
D_A	cm^2/s	4×10^{-7}	4×10^{-7}
λ_A	1/s	$4\times10^{-6,g}$	1.4×10^{-7}
A_r	-	1	1
k_A	1/s	1.65×10^{-6}	1.65×10^{-6}

[a] [92]

[b] estimated from [93]

[c] estimated using $\sigma_d = \left(1-(1-\alpha)^2\right)^2$ with ratio of drug to pore radius, $\alpha = 100$ nm/500 nm [94]

[d] diffusional permeabilities taken to be %5 of the effective permeabilities measured in [95]

[e] calculated using $P_d\frac{S}{V}$

[f] [96]

[g] [97]

Since the time scale of the tumor growth is much larger than the time scale for the transport and distribution of the drug molecules, both antiangiogenic agent and chemotherapy drug equations are solved in steady state, i.e. $\frac{\partial d(\mathbf{x},t)}{\partial t} = \frac{\partial A(\mathbf{x},t)}{\partial t} = 0$.

Both drugs are administered to the plasma with bolus injection in each administration through an exponential decay function:

$$A_v(t) = A_0 e^{-t/t^A_{1/2}}, \tag{4.6}$$

$$d_v(t) = d_0 e^{-t/t^d_{1/2}}, \tag{4.7}$$

In these equations, the terms A_0, d_0 and $t^A_{1/2}$, $t^d_{1/2}$ indicate the peak plasma concentration and the plasma half-lives of the antiangiogenic agent and chemotherapy drug, respectively. No-flux boundary conditions are used for the antiangiogenic agent and the chemotherapy drug.

Parameters related to transport of interstitial fluid and transport of liposomes and antiangiogenic agents are listed in Table 4.1 and Table 4.2, respectively. Some of the effective parameters in the equations above dynamically change to mimic the changes in tumor and its microenvironment. As the tumor grows, lymph vessels are diminished to ensure that there are no lymph vessels inside the tumor. Without the presence of tumor, vessel density can increase up to a specific value (the dimensionless value of 1). When vessel density is greater than 1, it implies that they were produced by angiogenesis and leaky, thus their hydraulic conductivity is increased up to levels that is observed in tumors. During antiangiogenic treatment, vessel density is decreased and when it decreases below 1, normalization occurs and the hydraulic conductivity returns to normal tissue levels.

4.4. Results

We started the simulations with a small tumor (0.2 mm radius) and left it to grow for 30 days to an approximate radius of 13.5 mm. Vessels which were initially set as randomly distributed islands in the computational domain evolved into a heterogeneous state throughout the simulations due to the presence of tumor cells. Figure 4.1 shows

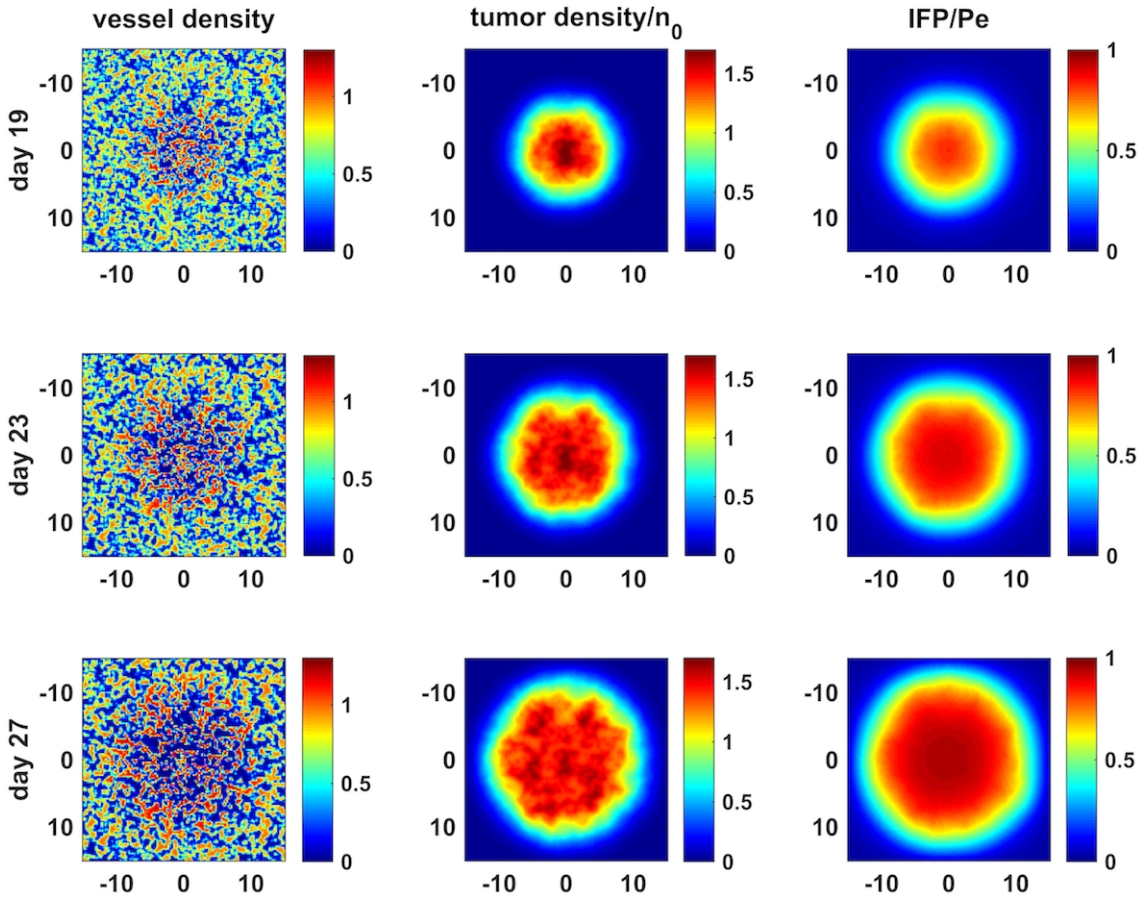

Figure 4.1. Control case showing vessel and tumor densities and IFP for days 19, 23 and 27.

vessel and tumor densities and IFP for contol case as time progress form day 19 to day 27. As the tumor grows, vessel islands become sparse in the interior region but their density increases by angiogenesis and they become leaky. By the end of the simulation, the leakiness of tumor vessels and the lack of lymphatic drainage inside the tumor causes elevated pressure in the interior region of tumor very similar to that suggested in literature [51, 53] (Figure 4.1, IFP/Pe).

We experimented with various drug regimens. To illustrate the improvement in drug delivery, we designed the cases given in Figure 4.2. From top to bottom, regimens for antiangiogenic agents alone (case-1), chemotherapy alone (case-2) and the combined therapy of antiangiogenic agents and chemotherapy drug (case-3 and case-4)

which show plasma concentrations for each drug over time.Dimensionless dose values are fixed in order to replicate the treatment response observed in [87]. Antiangiogenic treatment is adjusted such that at the end of administrations there is approximately a 50% decrease in MVD inside the tumor. A fixed chemotherapy drug dose is administered on days 23, 25 and 27 while we change the day of antiangiogenic agent administration starting from the days 15, 17, 19, 21 and 23, continue to give them every other day in 4 or 5 pulses. We decrease the dose of antiangiogenic agents throughout the therapy because a better response in drug delivery is obtained with this way in our simulations. We present here four cases where only antiangiogenic agent administration starts on day 23, only chemotherapy drug on day 23, neoadjuvant therapy with antiangiogenic agents on day 19 and chemotherapy drug on day 23 and finally concurrent therapy with both of drugs starting on day 23. The most beneficial results regarding the amounts of drugs extravasate in the interior parts of the tumor are yielded when the antiangiogenic treatment starts at day 19 (case-3 in Fig 4.2).

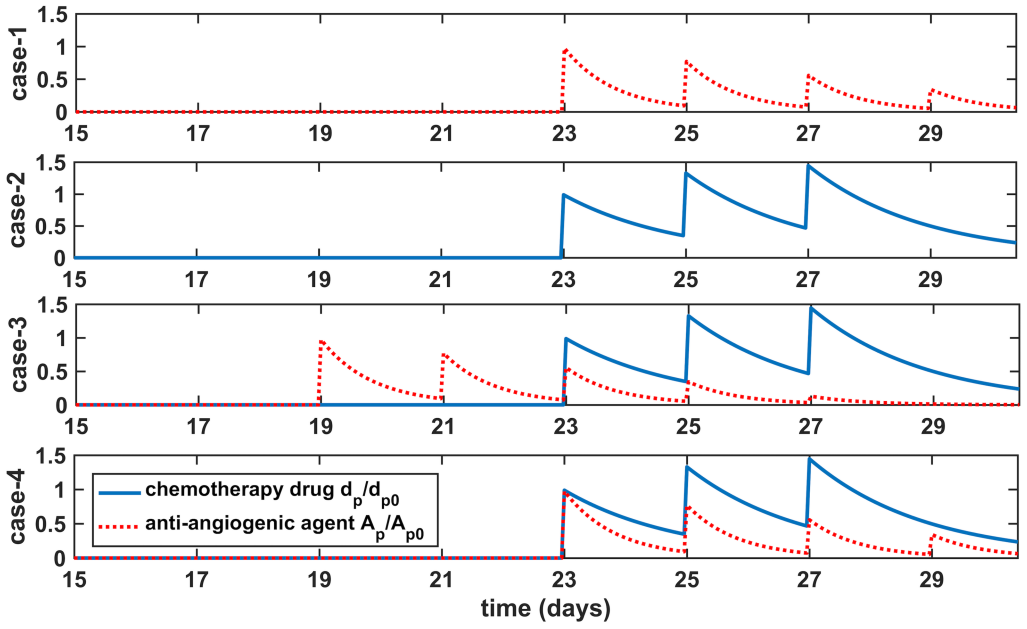

Figure 4.2. Drug regimens.

Tumor density and chemotherapy drug extravasation coefficient ($\Gamma_b(1-\sigma_d)$) are calculated for day 27 which corresponds with last application chemotherapy drug in Figure 4.4. As expected, antiangiogenic agents don't have a profound effect on tumor cell density when they are applied alone (Figure 4.4, case-1). In all cases, we observed greater drug extravasation near the tumor rim due to decreasing IFP in that region (Figure 4.4). It can be seen that fluid flow from vessels to the tumor is poor in the interior region for case-2, but it starts to enhance in the same region in case-3 and case-4. The main reason for this change is the introduction of a pressure gradient in the tumor center restoring drug convection. Therefore, in both case-3 and case-4, tumor cell density is decreased in the interior region (Figure 4.4 and Figure 4.4-b) as a consequence of increased drug extravasation in the interior region of the tumor.

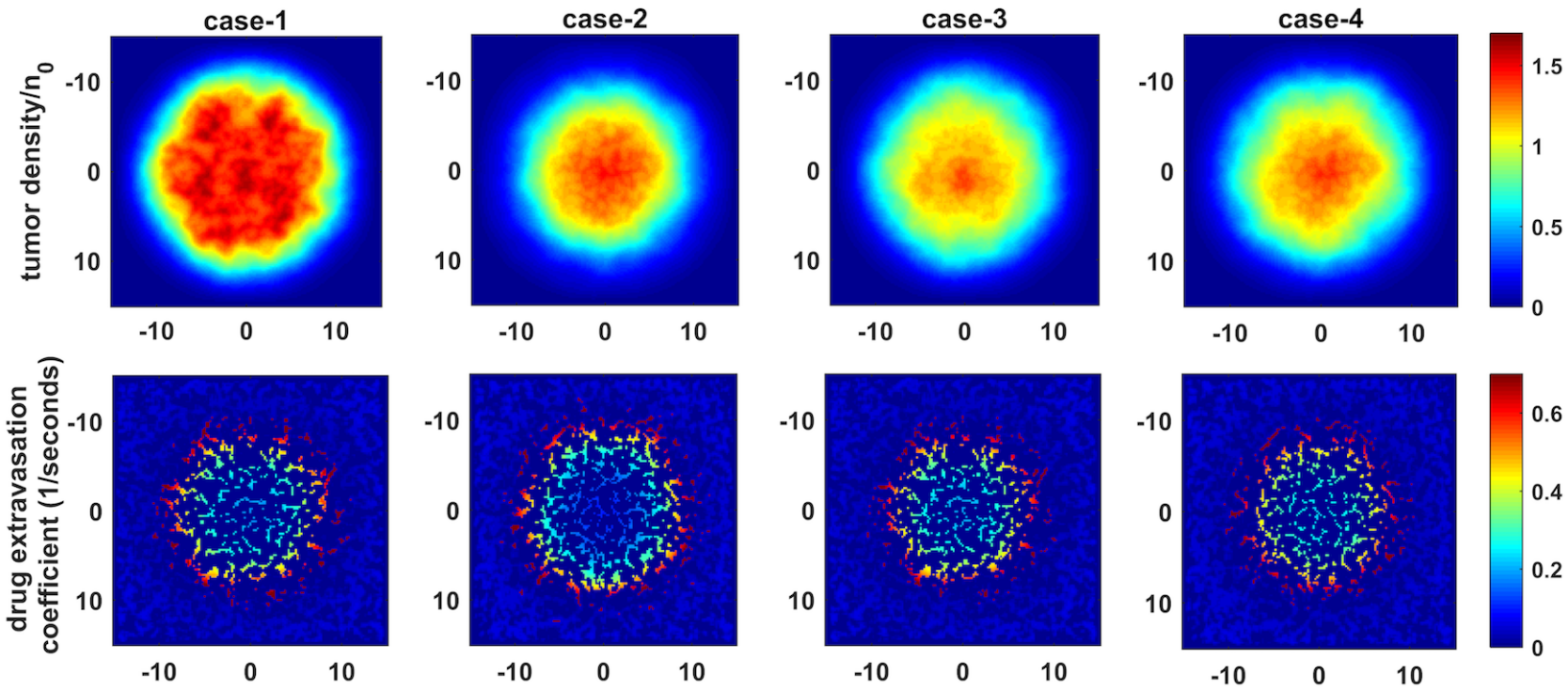

Figure 4.3. Tumor density and chemotherapy drug extravasation coefficient.

We calculate the space average of cell density and IFP in each time step. Average cell density is calculated as

$$\frac{\iint_{A_{int}} n(\mathbf{x}, \mathbf{y}, t)\, d\mathbf{x}\, d\mathbf{y}}{\iint_{A_{int}} d\mathbf{x}\, d\mathbf{y}} \tag{4.8}$$

over area A_{int} whose boundary is set by the condition $n(\mathbf{x}, \mathbf{y}, t) > 1$ which represents the interior region of tumor (corresponds to $r < 6$ mm for a tumor of radius 10mm). Average IFP is calculated as

$$\frac{\iint_{A} P(\mathbf{x}, \mathbf{y}, t)\, d\mathbf{x}\, d\mathbf{y}}{\iint_{A} d\mathbf{x}\, d\mathbf{y}} \tag{4.9}$$

over area A whose boundary is set by the condition $n(\mathbf{x}, \mathbf{y}, t) > 0.1$ which represents the value over whole tumor.

Equations 4.8 and 4.9 are used to calculate average IFP and average cell density, respectively in Figure 4.4. When we evaluate average pressure over the entire area of the tumor, we observe a synergistic effect in reducing pressure arising from the combined application of antiangiogenic agent and chemotherapy which can be seen in Figure 4.4-a, especially for case-4. This synergistic effect also exhibits itself in tumor cell density in a less pronounced manner that can be observed from Figure 4.4-b. This indicates improved combination treatment efficacy as an indirect result of decreasing IFP.

According to our results, drug extravasation from vessels in the interior region of the tumor is nearly doubled for combination cases (Figure 4.5-a, case-3 and case-4 compared to case-2). However, this improvement is not directly reflected on drug exposure due to reduced vessel density by antiangiogenic agents. Figure 4.5 shows drug extravasation rate from vessels and total drug exposure per unit area in the interior region of tumor by the end of the simulation. Total drug exposure of unit area in tumor during treatment only improves approximately 20-25%. IFP during the applications of chemotherapy drug was the lowest for concurrent therapy (case-4). However, regarding

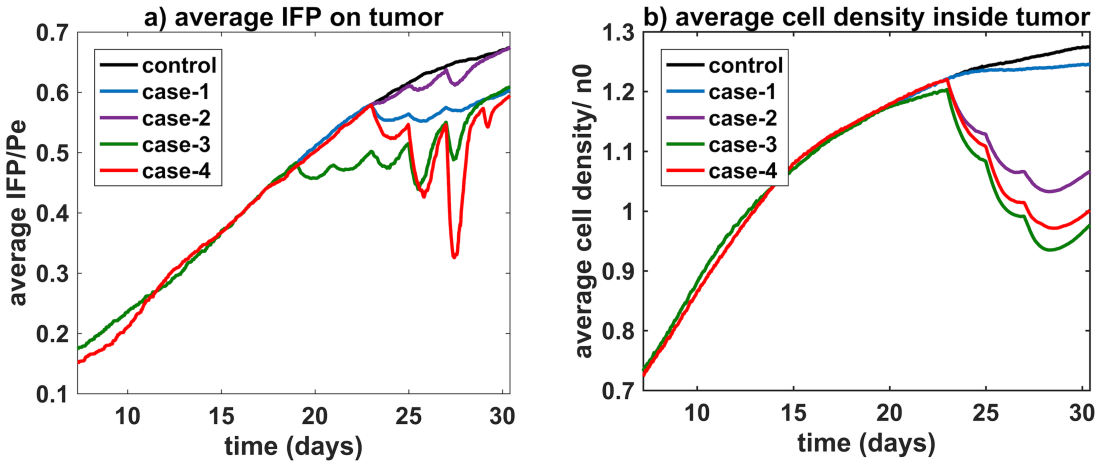

Figure 4.4. Average IFP over whole tumor and average cell density in the interior region of tumor.

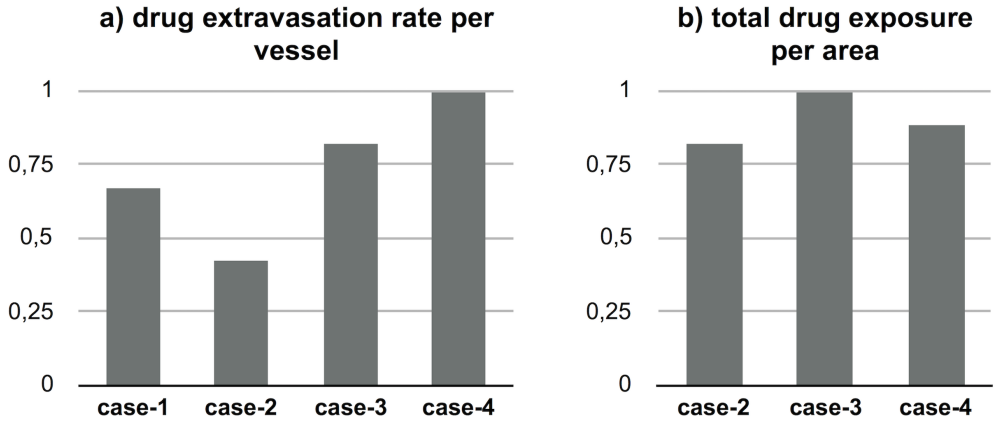

Figure 4.5. Drug extravasation rate from vessels and total drug exposure per unit area in the interior region of tumor by the end of the simulation.

tumor regression adjuvant therapy (case-3) performed better, agreeing with the results of Kohandel *et al.* [44].

Even though decrease in vessel density and leakiness cuts off the supply of drugs, the decrease in IFP appearing for the same reasons seems to compensate in the interior region of tumor, resulting in better drug extravasation. When two drugs are given closer temporally, the resulting IFP decrease is maximized. This enables the convective extravasation of nanoparticles deep into tumors to places that are not exposed to drugs without combination therapy.

In order to evaluate the effect of chemotherapy drugs that target tumor cell proliferation, we modified Equation 4.1 such that the chemotherapy drugs would directly act on tumor growth. The terms responsible for tumor growth (2nd and 3rd terms in the right-hand side of Equation 4.1 are multiplied by $(1 - d(x,t)/d_{max})$ where d_{max} is maximum drug concentration that extravasated inside the tumor. Figure 4.6 shows tumor density and chemotherapy drug extravasation coefficient $(\Gamma_b(1-\sigma_d))$ calculated for day 27 which corresponds with the last application of chemotherapy drug for the chemotherapy drugs that inhibit tumor growth. In this scenario, small changes are seen in tumor cell densities between combination therapy and chemotherapy alone. However, we observe that in this form, extravasation of drugs is also increased in the central region as seen in Fig4.6, implying that normalization is also beneficial in this scenario.

4.5. Discussion

Using a mathematical model, we assessed whether antiangiogenic therapy could increase liposome delivery due to normalization of tumor vessels. In order to do that, we first developed a dynamic vessel structure that exhibits properties of tumor vessels created by angiogenesis as well as inherent vessels in the tissue.

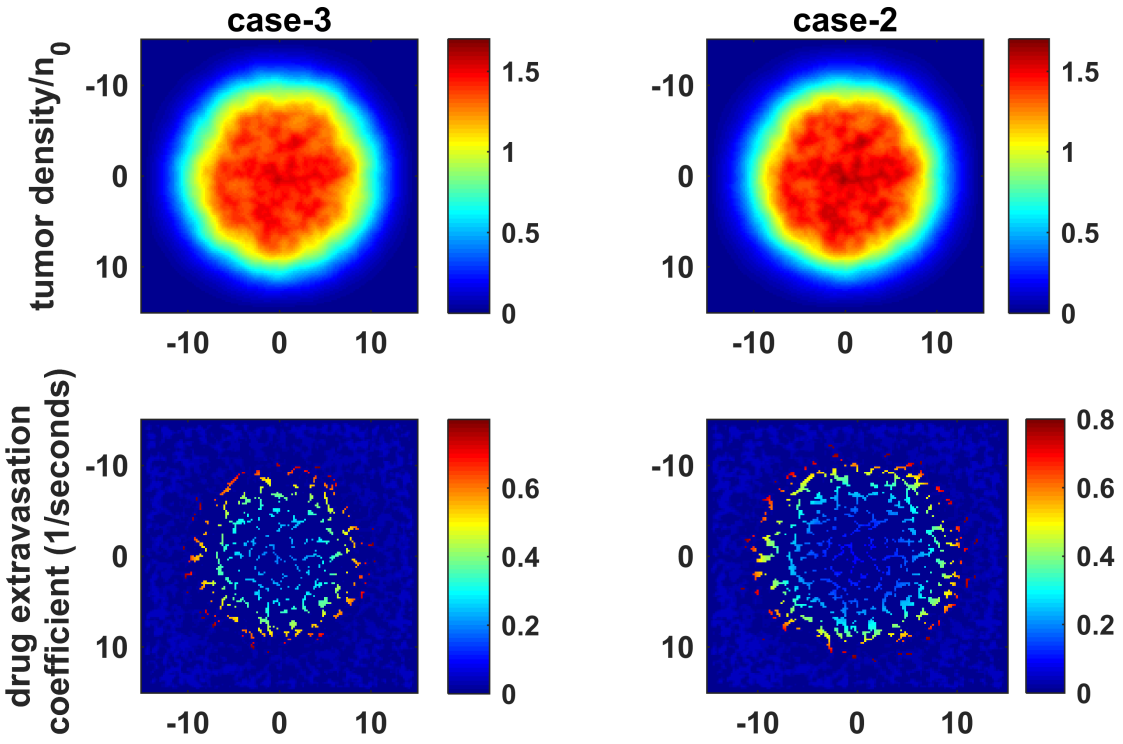

Figure 4.6. Tumor density and chemotherapy drug extravasation coefficient for drugs acting on tumor cell proliferation.

As the tumor grows, vessels in the central region begin to disappear due to increased tumor cell density in that region. Angiogenesis occurs in the tumor creating additional leaky vessels. The emergent vessel density is consistent with that observed in [98], with decreasing density towards the tumor center along with randomly appearing clusters of vessels. IFP is found to be elevated throughout the tumor up to the levels of MVP and decreases sharply around the tumor rim as it is observed in various studies in the literature [51, 53, 54].

We apply antiangiogenic agents in various regimens combined with chemotherapy and focus on large drugs (liposomes) whose delivery mainly depends on convection. As a result of the decrease in vessel density and leakiness due to the antiangiogenic activity, we expect a decrease in pressure which brings about a higher pressure difference between tumor and vessels. Transvascular convection depends on this pressure difference, hydraulic conductivity and density of vessels at the unit area. Since antiangiogenic agents decrease hydraulic conductivity (i.e. leakiness) and vessel density, by cutting the supply of drugs, the resulting increase in pressure difference should compensate for these effects, restoring extravasation in remaining vessels.

In all simulations, liposome extravasation predominantly occurs in the tumor periphery due to low IFP levels in this area, hence drugs preferentially accumulate in there. Our result has been confirmed by experimental studies of drug distribution using large drugs such as micelles [99, 100], nanoprobes [101] and liposomes [98, 102–105] in which peripheral accumulation of large drugs is observed.

As the application time between antiangiogenic agents and liposomes becomes shorter, the resulting decrease in IFP is maximized. This enables the convective extravasation of nanoparticles deep into tumors to places that could not previously be exposed to drugs before and liposome extravasation begins to appear in central region. However, that does not bring about maximum accumulation of liposomes consistently at all times. There is a trade-off between total drug accumulation and how deeply drug can penetrate inside the tumor.

In our study, we find a balance between these two situations. It also shows us that IFP and drug accumulation are not always correlated, rather the maximum accumulation is achieved through the complex interplay between IFP, vessel density and leakiness. Current research by Stapleton *et al.* also supports this view; in their mouse study, they point out that IFP is correlated with blood perfusion, blood perfusion is correlated with liposome accumulation and the relationship between IFP and liposome accumulation is limited [102].

In another significant study, tumor-bearing animals are subjected to combination therapy with liposomes and the antiangiogenic agent pazopanib in order to evaluate the effect of normalization via imaging drug distribution [104]. As a result of the decrease in MVP, they also observed a resulting decrease in IFP. Similar to our results, IFP is not the determinant of drug accumulation in their work. They have found that decreased leakiness of vessels inhibits delivery even though there is an IFP decrease as a result of antiangiogenic therapy. They have collected data for a single time point and observed a decrease in doxil penetration in combination therapy. They also point out that functional measures of normalization may not occur simultaneously which is also the case for our study. Throughout the combination therapy, we also observe periods where drug extravasation is limited and others where drug extravasation is improved. They have found the vessel permeability as a limiting factor in their study, however MVD [106] and tumor blood flow and blood volume [107] are also determinants of large drug accumulation. This shows that these measures of normalization are tumor type dependent and even within the same tumor they are dynamic which leads to variation in drug distribution.

Among many different schedules, most of our trials did not show improvement in drug accumulation. We see that the dose of antiangiogenic agents should be carefully determined to ensure any delivery benefit. As stated by [74], when we apply a large dose of antiangiogenic agents, significant IFP decrease is observed but the decrease in vessel permeability and the lack of vessel density lead to impaired liposome extravasation.

At the other extreme, when we give small amounts of ant-angiogenic agents, it is seen that IFP decrease is not enough to make a significant improvement to liposome extravasation.

In this model, intravascular flow is approximated as uniform to focus on the effects of transvascular delivery benefit of normalization. Due to abnormal vasculature, tumors are known to have impaired blood perfusion [108] because of the simultaneous presence of functional and non-functional vessels. In this work, we simulate structural normalization of vessels without considering functional normalization which is associated with intravascular flow and results in increased perfusion [74]. Vessels within the tumor in this model have uniform functionality in terms of supplying blood flow. Hence, by decreasing vessel density in microenvironment due to antiangiogenic activity, we are decreasing blood perfusion. However, on the contrary, normalization is expected to enhance intravascular flow by decreasing pore size which restores intravascular pressure gradients and pruning non-functional vessels that interrupt circulation. Therefore, normalization brings about improved blood perfusion whereas here we decrease perfusion and improve the delivery only through improved convective extravasation by decreased IFP. In our simulations, the delivery benefit is underestimated since we decrease blood perfusion as a part of antiangiogenic activity. In [104], they observed that MVD decrease did not change liposome accumulation because the eliminated vessels are the ones that are thought to be nonfunctional. In our previous study, we constructed a spherical tumor with uniform vessel density to investigate the benefit from normalization therapy and the results showed increased delivery in the interior regions of tumors of certain sizes [109].

In animal studies, it has been shown that the bulk accumulation of liposomes is not representative of efficacy since it is not informative about the drug accumulation within specific regions of tumors [106, 110] and heterogeneous drug accumulation may result in tumor repopulation [111]. Therefore, it is important to understand the factors that yield heterogeneous accumulation and strive to avoid them to generate effective treatments.

According to our results, it is plausible that administering targeted therapies using large drugs, normalization should be more useful since it can provide a simultaneous access to both tumor rim and center. The dose of chemotherapy should be increased in order to ensure similar drug exposure despite the sparser vessel density caused by antiangiogenic activity. This is the reason why targeted therapies are more suitable to seize the benefits from normalization, as they can be applied in greater doses without harming healthy tissue. When convective extravasation is restored in the central region, drugs can immediately reach to tumor center and increase the probability of treatment success and tumor eradication.

5. PROANGIOGENIC TREATMENT STRATEGIES TO ENHANCE DRUG DELIVERY AND TREATMENT RESPONSE

Angiogenesis, which is triggered and governed predominantly by the members of the vascular endothelial growth factor (VEGF) and angiopoietin (Ang) family, plays a significant role in tumor growth and cancer cell metastasis. Tumors utilize angiogenesis to form a vascular network that provides oxygen and nutrients supply tumor cells need to grow. VEGF is present in high concentrations around tumor blood vessels and hypoxic regions. Besides inducing angiogenesis, VEGF leads to hyper-permeable tumor blood vessels by enlarging pores and loosening the junctions between the endothelial cells that line the capillary wall [112–114]. Angiogenesis is a major component contributing the abnormalities in the tumor microenvironment. These abnormalities not only sustain the microenvironmental conditions that increase malignancy, but they also create difficulties in drug delivery [3, 13].

Due to its role in cancer progression, angiogenesis is a target for therapy. Conventional antiangiogenic therapies, composed of vascular disrupting agents and angiogenesis inhibitors used to combine with chemotherapy or alone to starve tumors. However, the interaction of angiogenesis inhibitors with tumor microenvironment is complex, making clinical success unreliable. Nevertheless, advancements appear for antiangiogenic agents that provide the opportunity to utilize them in therapy in new ways.

Studies have shown that the down-regulation of VEGF signaling by using antiangiogenic agents can remodel the tumor vasculature, restoring some normal function and structure, a process referred to as vascular normalization [2, 3]. During vascular normalization, blood flow to the tumor is improved at the expense of reducing tumor blood vessel density. In combination with chemotherapy, vascular normalization can result in better blood perfusion and drug delivery and controlled tumor growth [4,115,116]. This

state is transient since it depends on the balance between the proangiogenic and antiangiogenic factors, hence, to seize its benefits in clinical settings, treatment scheduling and the dose of antiangiogenic agents should be adjusted accordingly.

A novel approach for targeting tumor vasculature, asserting that the stimulation of tumor angiogenesis may have synergistic effects when combined with chemotherapy, is called vascular promotion therapy. In this approach, contrary to the vascular normalization, the density of tumor blood vessels is increasing. The idea behind it comes from the evidence concerning the agonistic effect of RGD-mimetic integrin inhibitors [27, 28, 117]. They are shown to increase vessel density and tumor growth by increasing angiogenesis [27]. Cilengitide, an antiangiogenic drug that targets integrins $\alpha_v\beta_3, \alpha_v\beta_5$ and $\alpha_5\beta_1$ [118] has exhibited proangiogenic effects when applied in low doses [27]. Therapy with low-dose cilengitide is observed to increase VEGF mediated angiogenesis [27–29, 119] which is associated with an increase in the recycling and signaling of the VEGFR-2 [119].

Enhancement in drug delivery with the help of pro-angiogenic drug has been demonstrated for small chemotherapy drugs. According to a recent experiment conducted on mouse using lung and pancreatic cancer models in vivo, it is stated that using low-dose Cilengitide and Verapamil increased tumor angiogenesis and leakiness resulting in an increase in the delivery of chemotherapeutic agent Gemcitabine [29]. This strategy provided substantial benefits for cancer therapy such that it decreased tumor size dramatically compared to only Gemcitabine application.

In this work, it is aimed to explore the potential benefit of vascular promotion in drug delivery and its effects on the tumor microenvironment and ultimately on the treatment response by building a mathematical model simulating tumor and its microenvironment. Proangiogenic drugs are applied to tumor-vessel growth model to simulate vascular promotion in combination with conventional and large chemotherapy drugs to achieve chemotherapy drug delivery and treatment response benefit.

Proangiogenic drugs can lead to changes in the dynamics of tumor microenvironment in many ways. We expected to have greater vessel density which would aid both diffusion and perfusion limited delivery of drugs. This could also decrease the regions of hypoxia, making tumor cells more responsive to therapy. On the other hand, by proangiogenesis, we are supplying the rapidly dividing tumor cells with more nutrients making the tumor growth escalate. Microenvironmental abnormalities such as leaky vessels produced by angiogenesis and lack of functional lymphatics inside the tumor cause IFP to elevate within the tumor. Increasing the blood vessel density and leakiness by proangiogenesis would result in a further increase in IFP which is already high inside the tumor. Eventually, we expect to see a decrease in transvascular and intratumoral convective transport. Considering all these factors, enhancement in drug delivery by proangiogenic agents is worth investigating further since drug delivery inside the tumor had to be subject to physical rules of transport.

5.1. Related Literature Review in Modeling of Tumor

Targeting vessel growth in the context of its synergistic effects with therapy has been studied with the help of mathematical models previously in the literature. d'Onofrio and Gandolfi proposed a model for chemotherapy considering the interaction between tumor and vessel growth [120]. They have found multi-stability in solutions for continuous administration of drugs which may account for failures in therapy and for periodic administrations of the drug, the possibility of the existence of an optimal delivery frequency that minimizes the average tumor volume. In another study, a cylindrical tumor cord around the vessel is modeled to focus on the effect of different drug regimens and the changes in drug dose and binding, and vessel properties on the tumor exposed to Doxorubicin [121]. Jain *et al.* modeled IFP inside the tumor and analyzed the microenvironmental conditions that can lower IFP to increase drug delivery [32]. In addition to that, physical barriers to drug delivery and mathematical models concerning this subject which proposed treatment strategies for better drug delivery are reviewed in a study by Stylianopoulos *et al.* [122]. To work on this subject, we build a mathematical model based on our previously proposed model with coupled partial dif-

ferential equations (PDEs) representing the change in biological components in tumor microenvironment [123]. In that previous framework, the conditions in which tumor vessel normalization yielded therapeutic benefit by enhancing drug delivery were determined. Chemotherapy strategies including their interactions with vasculature studied mathematically also in the literature to find the limitations of the tumor-vasculature system on drug delivery and treatment response.

5.2. Mathematical Model

In this model, a novel approach is taken to explore the effect of proangiogenesis on vessel structure. Dependence of angiogenesis to VEGF density is built into the model equations. Proangiogenic and chemotherapy drugs are applied to the system to be informed about their synergistic effects on drug delivery. To capture the impact of proangiogenesis in the distinct transport mechanisms for different sizes of chemotherapy drugs, we picked two types of chemotherapy drugs representing large and small sizes to exemplify the main transport mechanism as convection and diffusion, respectively.

We observed that combining proangiogenic drugs with chemotherapy can enhance tumor regression compared to only chemotherapy application and this synergistic effect is achieved through the better delivery of chemotherapy drugs. It is found that the faster drug acts on the tumor cells, the more significant difference in treatment outcomes occurs between these two cases. According to our results, for this scenario to be successful for large chemotherapy drugs, the chemotherapy drug should decrease the tumor cell density enough to lower IFP below microvascular pressure (MVP) in the early stages of therapy. We studied proangiogenic therapy on tumors with high and low vessel densities and found that tumor regression is similar for tumors with different vessel configurations.

5.3. Model Equations

In this study, we build a mathematical model following our previously proposed model where biological components in the tumor microenvironment are changing in time due to biological processes and their coupled interactions [123]. Non-linear PDEs are employed for each component to determine these changes. The system of equations is solved by adopting the finite difference method for PDEs. Details about solution method can be found in Chapter 3.

5.3.1. Tumor cells, vasculature, and IFP

Equation 5.1 governing the change of tumor cell density ($n(x,t)$) was taken from our previous mathematical model [123]. It includes diffusion of tumor cells, the growth of the tumor cells up to the carrying capacity of the microenvironment, vasculature driven growth and destruction of vessels by chemotherapy drugs ($d_i(x,t), i = \{1,2\}$) in the right-hand side, respectively. Initial tumor density is set up as a Gaussian distribution.

$$\frac{\partial n(x,t)}{\partial t} = D_n \nabla^2 n(x,t) + r_n n(x,t)(1 - \frac{n(x,t)}{n_{lim}}) + \alpha_{mn} n(x,t) m(x,t) - d_{ir} n(x,t) d_i(x,t), \tag{5.1}$$

where $d_1(x,t)$ and $d_2(x,t)$ represent small and large drugs, respectively.

We constructed vessel density equation (Equation 5.2) to create a heterogeneous vessel structure with an increased vessel density in the tumor periphery and a hypo-vascular tumor core [124] due to the collapse of vessels in there with the increased solid pressure and IFP [88]. Vessel islands ($m(x,t)$) are produced by the second term in the right-hand side which is introduced in the mathematical model of tumor growth by Kohandel *et al.* [44]. The term collapses the equation to the two stable points at $m = 1$ and $m = 0$ and one unstable point at $m = 1/2$, creating vessel islands in the computational domain. Development of vascular structure in the tumor microenvironment is enhanced by angiogenesis which is dependent on VEGF availability.

Angiogenesis is represented in the third and fourth terms where the vessels are produced in the presence of VEGF ($V(x,t)$) and move through the interior regions of the tumor, respectively. The last term is recruited for generating the sparsity of vessels due to vascular collapse. It is fixed to have nonzero for values of $n(x,t)$ greater than n_{lim}. For that range, it attains negative values to eliminate the overgrowth of the vessels. Vessel density is initiated as a map of random numbers between 0 and 1. Parameters related to tumor growth can be found on Table 5.1.

$$\frac{\partial m(x,t)}{\partial t} = D_m \nabla^2 m(x,t) + m(x,t)(\alpha + \beta m(x,t) + \gamma m(x,t)^2) + \alpha'_{nm} n(x,t) V(x,t) + \beta'_{nm} \nabla.(m \nabla n) - r_m \frac{n(x,t)}{n_{lim}} m(x,t). \quad (5.2)$$

VEGF which is essential for angiogenesis is initially produced by tumor cells with the second term in the right-hand side of Equation 5.3. Without the application of proangiogenic drugs, VEGF density can increase up to the values that could enhance the vessel density to a limiting value m_{max}. When the proangiogenic drug is present, VEGF density is increased in the tumor microenvironment (the third term in Equation 5.3). g_V is the constant rate of production which is equal to $2x10^{-4} mg/mm^3 s$ and $12x10^{-4} mg/mm^3 s$ in healthy tissue and in tumor, respectively [45]. VEGF density is initially zero in the computational domain, and it is set to build up as the tumor grows. In simulations, steady state of VEGF equation is solved since its evolution is faster compared to timescales associated with tumor and vessel growth ($\frac{\partial V(\mathbf{x},t)}{\partial t} = 0$).

$$\frac{\partial V(x,t)}{\partial t} = D_V \nabla^2 V(x,t) + g_V (1 - \frac{m(x,t)}{m_{max}}) V(x,t) + A_V V(x,t) A(x,t) - k_v V(x,t). \quad (5.3)$$

Leakiness of tumor vessels and lack of functional lymphatics inside the tumor [90] lead to an increase in interstitial fluid pressure within the tumor governed by Equation 5.4. Interstitial flow (IF) is proportional to gradient of IFP and steady-state mass continuity guaranties that divergence of IF which is equal to Laplacian of IFP (Equation 5.4, term on the left hand side) is given by the difference of the supply of fluid from blood vessels (first term on right-hand side) and the collection of fluid by lymphatic

Table 5.1. Dimensionless tumor and vessel growth parameters.

Parameter	**Value**	**Parameter**	**Value**
r_n	0.75	n_{lim}	1.5
α_{mn}	1.15	r_m	0.7
α'_{nm}	1	β'_{nm}	0.5

system (second term in right-hand side). In simulations, lymphatics are only available at tumor boundary and outside the tumor.

Detailed derivation of Equation 5.4 can be found in Chapter 3. Initial and boundary values are set to its normal tissue value P_0.

$$-K\nabla^2 P(\mathbf{x},t) = \lambda_b m(\mathbf{x},t)\left[P_v - P(\mathbf{x},t) - \sigma_v(\pi_c - \pi_i)\right] - \lambda_\ell P(\mathbf{x},t). \tag{5.4}$$

Here, we related hydraulic conductivity of tumor vessels to the density of tumor cells according to relation given by Equation 5.5 to make it heterogeneous. This relation derived from [125], in that, dimensionless pamater $\alpha = R\sqrt{L_p S/KV}$, which determines the shape of IFP profile found by Jain et al. [32] is used to make hydraulic conductivity of vessels heterogeneous,

$$\lambda_b = H_n \exp(5n(x,t) - 3) \tag{5.5}$$

where H_n is equal to hydraulic conductivity of normal vessels.

5.3.2. Proangiogenic and chemotherapy drugs

In the model, a proangiogenic drug that shows the properties of small size drug is chosen. To scrutinize the effect of proangiogenic therapy on chemotherapy drug delivery, small and large size chemotherapy drugs are used. Doxorubicin is used to represent small drugs and $100nm$ liposomes are used to represent large drugs.

Proangiogenic drugs administered to blood plasma extravasate and are distributed through tumor interstitium by diffusion in the second and first terms of the right-hand side of Equation 5.6, respectively. The last term is responsible for the decay of the drug in the tumor interstitium. Transport parameters for proangiogenic drugs can be found in Chapter 4, Table 4.2.

$$\frac{\partial A(x,t)}{\partial t} = D_A \nabla^2 A(x,t) + \lambda_A m(x,t)(A_p - A(x,t)) - k_A A(x,t). \tag{5.6}$$

Proangiogenic drugs are known to increase the leakiness of tumor vessel, so when they are available, the relation determining the hydraulic conductivity in Equation 5.5 is modified to account for that increase.

$$\lambda_b = H_n \exp(5n(x,t) - 3) + k_\lambda A(x,t). \tag{5.7}$$

Main modes of transport which are dictated by Peclet Numbers are different for small and large drugs. For small drugs, diffusion overweights convection in the tumor microenvironment. Hence, the small drugs ($d_1(x,t)$) are modeled to diffuse through vessels and tumor interstitium in the second and first term in the right-hand side of Equation 5.8, respectively. Then, they react with tumor cells by the third term and decay in microenvironment by the fourth term. Transport parameters of small chemotherapy drug Doxorubicin is used to represent small drugs which are given in Table 5.2.

Table 5.2. Transport parameters of small chemotherpy drug Doxorubicin.

Parameter	**Healthy Tissue**	**Tumor**	**Unit**
D_1	$1.58x10^{-10}$	$3.4x10^{-10}$	m^2/s
λ_1	$3.75x10^{-7}$	$2.4x10^{-6}$	m/s

$$\frac{\partial d_1(x,t)}{\partial t} = D_1 \nabla^2 d_1(x,t) + \lambda_1 m(x,t)(d_{1p} - d_1(x,t)) - d_{1r} d_1(x,t) n(x,t) - k_1 d_1(x,t). \tag{5.8}$$

For large drugs ($d_2(x,t)$), convection is the main mode of transport since their diffusion is slower. Drugs extravasate by convection given by the third term in the right-hand side of Equation 5.9. Then they diffuse and convect through the interstitium by the first and second terms, respectively. Following terms represent the collection of drugs with the lymph vessels around the tumor, reaction with tumor cells and drug decay. $100nm$ liposomes are used to represent large drugs. Transport parameters of liposomes can be found in Chapter 4, Table 4.2.

$$\frac{\partial d_2(x,t)}{\partial t} = D_2\nabla^2 d_2(x,t) + \nabla\cdot(k_E d_2(x,t)K\nabla P) + \Gamma_b d_2(x,t)(1-\sigma_2) - \Gamma_l d_2(x,t) - d_{2r}d_2(x,t)n(x,t) - k_2 d_2(x,t). \quad (5.9)$$

In Equation 5.9, transvascular blood flow in convection term is represented by $\Gamma_b = \lambda_b m(\mathbf{x},t)\left[P_v - P(\mathbf{x},t) - \sigma_v(\pi_c - \pi_i)\right]$, and fluid flow to lymph vessel is represented by $\Gamma_\ell = \lambda_\ell P(\mathbf{x},t)$.

Since the time scale associated with their movements are shorter than that of the main equations of the model like tumor and vessel growth, all drug equations are solved for steady state ($\frac{\partial d_i(\mathbf{x},t)}{\partial t}, \frac{\partial A(\mathbf{x},t)}{\partial t} = 0$).

Chemotherapy drugs are given to blood stream in bolus injections in days 23, 25, and 27. Proangiogenic agents are given either together or before the administration of chemotherapy drugs in bolus injections. Bolus injections in plasma are determined by exponentially decaying functions $A_p(t) = A_0 e^{-t/t^A_{1/2}}$, and $d^i_p(t) = d^i_0 e^{-t/t^{d_i}_{1/2}}$, where A_0, d^i_0, and $t^A_{1/2}, t^{d_i}_{1/2}$, indicate the peak plasma concentration and the plasma half-lives of the proangiogenic agent and chemotherapy drugs, respectively.

5.4. Results

To explore the benefit from proangiogenic drugs, we tried giving them before the onset of chemotherapy and during chemotherapy. The most significant improvement in tumor regression is observed when proangiogenic, and chemotherapy drugs are given

together (concurrent therapy). We present the simulations of six cases that demonstrate the effect of proangiogenic drugs which are summarized in Table 5.3.

Table 5.3. Proangiogenic drugs and chemotherapy combinations.

Cases	**Drug combinations**
(I)	Control case - no drugs
(II)	Only proangiogenic drugs
(III)	Only large chemotherapy drugs
(IV)	Concurrent combinations of proangiogenic and large chemotherapy drugs
(V)	Only small chemotherapy drugs
(VI)	Concurrent combinations of proangiogenic and small chemotherapy drugs

Concurrent therapy simulations are conducted on tumors having high and low vessel densities to understand their effects on tumors with different microenvironmental conditions. Simulations include (I) control case where no drug applications on tumor, (II) only proangiogenic drugs applications, (III) only chemotherapy with large drugs (LD) applications, (IV) concurrent applications of both proangiogenic drug and chemotherapy with LD, (V) only chemotherapy with small drug (SD) applications and (VI) concurrent applications of both proangiogenic drug and chemotherapy with SD which are summarized in Table 5.3. Simulation results for these cases at the end of day 30 are shown in Figure 5.1 and Figure 5.2 for high and low vessel densities, respectively.

In our simulations, drug delivery enhancement from proangiogenic agents resulted in more tumor cell eradication in concurrent therapy (IV and VI in Figure 5.1 and Figure 5.2) compared to chemotherapy alone (III and V in Figure 5.1 and Figure 5.2). However, a more developed vasculature resulting from proangiogenic agents provided a faster tumor growth, these two opposite effects competed with each other and brought about a similar regression in tumors having only chemotherapy and concurrent therapy.

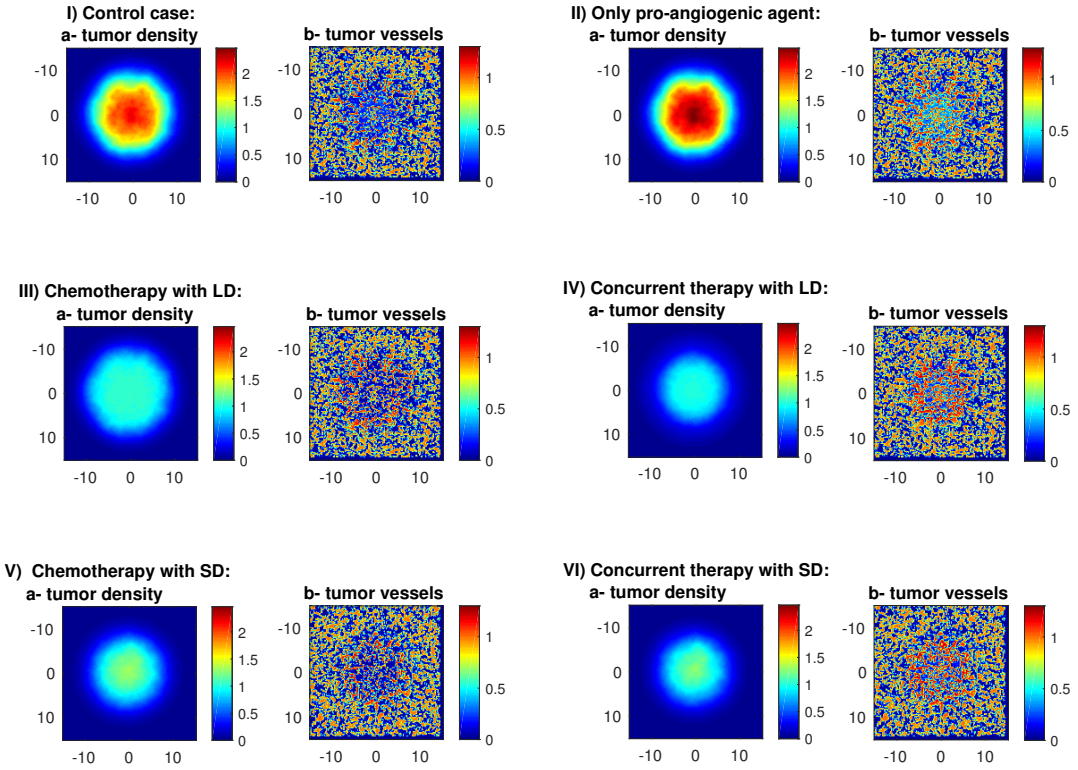

Figure 5.1. Tumor cell and vessel density for tumors with high vessel density.

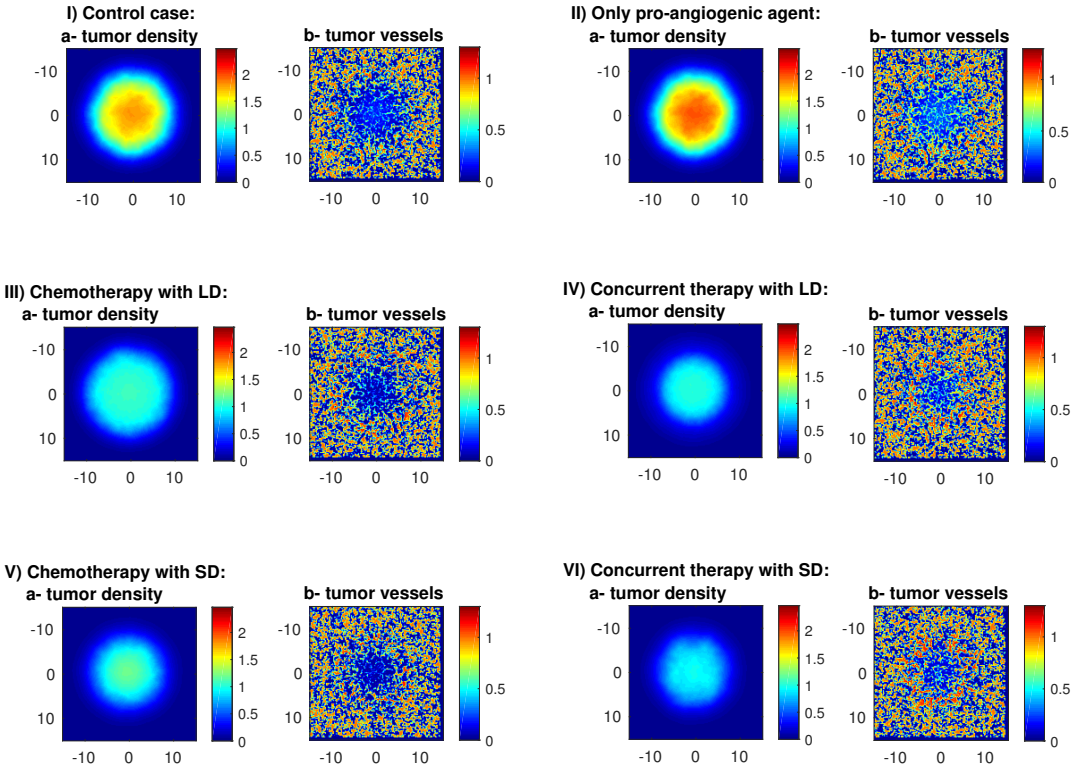

Figure 5.2. Tumor cell and vessel density for tumors with low vessel density.

To see an increase in tumor regression in concurrent therapy compared to chemotherapy alone, we increased the reaction rate of chemotherapy drugs with tumor cells. By the increased reaction rate, the enhancement in regression between these two cases (III vs. IV and V vs. VI) becomes more pronounced. Therefore, we concluded that aggressive chemotherapy drugs worked better with proangiogenic strategies.

Total number of tumor cells are measured through treatment period until the end of simulations on day 30 in tumors with a) high and b) low vessel density for six different cases (I-VI) are shown in Figure 5.3 Percentage improvement in tumor regression was almost the same for tumors with high and low vessel densities (Figure 5.3). For all the six cases presented here (I-VI), we observed around 30% decrease in total tumor cell number at the end of concurrent therapy (case-IV) compared to chemotherapy with large drugs (case-III) and around 15% decrease at the end of concurrent therapy (case-VI) compared to chemotherapy with small drugs (case-V).

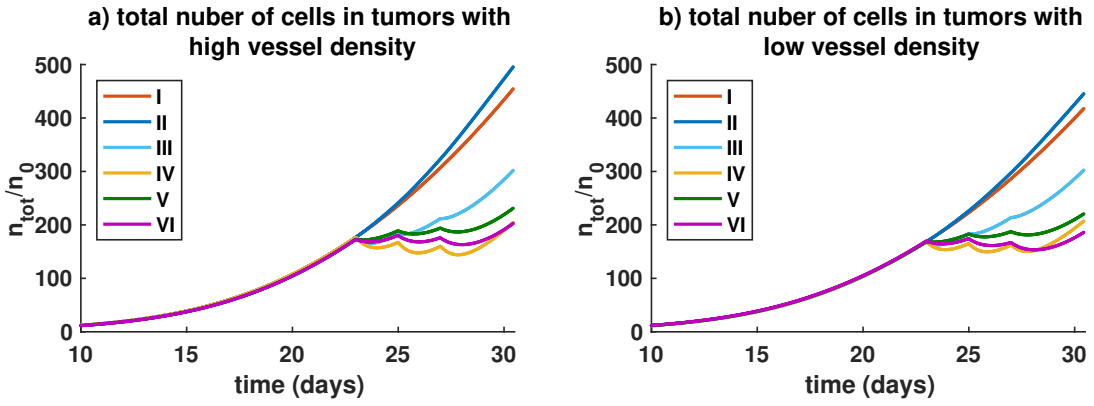

Figure 5.3. Total number of tumor cells in time.

IFP is measured along the radial distance from tumor center (corresponds to 0 in the x axis) at day 26, which is the middle of the treatment period. IFP is captured in tumors with a)high and b)low vessel density for six different cases (I-VI) in Figure 5.4. We observed the well-established high IFP plateau at pressure equal to MVP in the center of tumor ([51, 126]) in tumor with high vessel density and a lower IFP profile reaching around MVP value in tumor center for low vessel density in associated control cases (case-1 of a) and b) in Fig 5.4). As expected, adding the proangiogenic agent to therapy scenarios increased IFP (I vs. II, III vs. IV and V vs. VI in Figure 5.4). However, this increase was not enough to eliminate the drug delivery improvement proangiogenic agents provide.

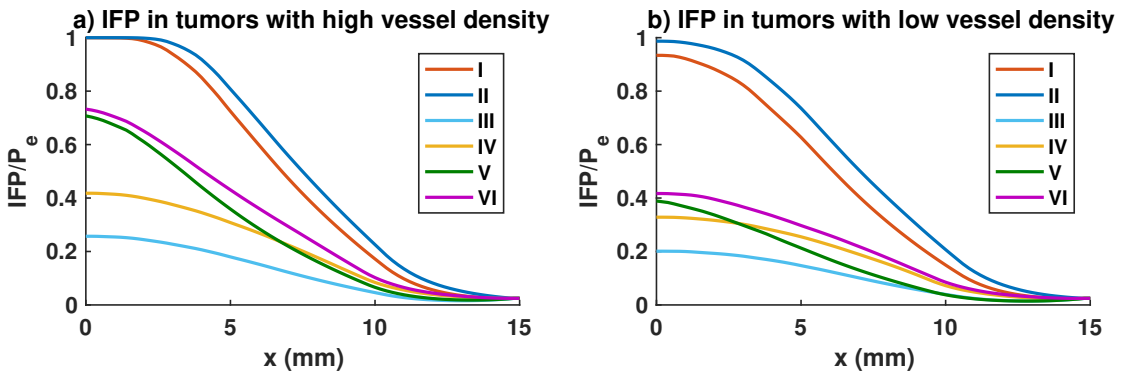

Figure 5.4. IFP along the radius of tumor.

5.5. Discussion

Proangiogenesis that is occurred via applications of low concentrations $\alpha_v\beta_3/\alpha_v\beta_5$ inhibitors have been shown to increase VEGF mediated angiogenesis [27, 28] resulting in tumor growth indirectly by increasing vessel density [27]. Accordingly, we construct the relations governing the increase in tumor density in connection with vascular growth (Equation 5.1) to observe this indirect effect.

In vessel density equation (Equation 5.2) angiogenesis is connected to VEGF content. Proangiogenic agents increase this VEGF content in our model in compliance with observations in literature, to further increase the vessel density. Vessel density varies among different tumors, and the degree of vascularization of tumor relates to clinical outcome [127]. We analyzed how the initial configuration of vessels affect the progress of therapy by creating highly and poorly vascularized tumors by adjusting our model. We found that for tumors with high and low vessel density proangiogenic drugs prove to be more helpful in decreasing the tumor density compared to chemotherapy alone. Furthermore, the difference in treatment outcomes was merely the same for tumors having high and low vessel densities.

Consistent with our results, increase in vessel density during therapy shown to be associated with better outcome in the work of McCormack *et al.* [128]. In breast cancer xenografts experiments with trastuzumab shown that tumors responsive to the drug showed increased vessel density by the action of the drug. There was a correlation with response to the drug with vessel density. Wong *et al.* [29] demonstrated many benefits of vascular promotion in their work on mice. They showed that Gemcitabine delivery increased in Lewis lung carcinoma and pancreatic cancer making treatment more efficient by application of proangiogenic doses of Cilengitide and vasodilator Verapamil. They stated that delivery is increased even in the center of the tumor which is also consistent with our findings. In Figures 5.1 and 5.2, it can be seen that in combination therapy cases tumor density is lower in tumor center compared to only chemotherapy application case.

Proangiogenic therapy has the potential to reduce hypoxia which leads to treatment resistance in tumors. This resistance is one of the main reasons for unfavorable outcomes from treatments and can trigger mechanisms that lead to tumor regrowth [30]. Decrease in hypoxia by proangiogenic therapy is observed in Wong *et al.* [29].

It was surprising to see proangiogenic drugs can have synergistic effects enhancing therapy outcome when large chemotherapy drugs are used. We expect it to be challenging since in that case, IFP would be high enough to inhibit extravasation of large chemotherapy drugs. However, we observed that if the chemotherapy drug reacts fast and decreases the density of tumor cells sufficient to reduce IFP to sub-MVP levels, enhancement in drug delivery occurs (cases III vs. IV and VI vs. V in Figure 5.1 and Figure 5.2).

It is reasonable to conceive that if IFP profile has reached to its maximum attainable value MVP and above MVP levels and has a steep curve, to effectively discard large drugs from blood vessels, IFP needs to fall below MVP levels to sustain convective transport across vessels. The relationship of IFP profile with tumor parameters are derived in work by Jain *et al.* [32]. They formed a parameter α determining the shape of IFP profile such that $\alpha = R\sqrt{L_p S/KV}$ where K is the tissue hydraulic conductivity, L_p is the hydraulic permeability of vessels and S/V is the surface area of vessel wall per unit volume of tissue. Keeping other parameters constant Ozturk *et al.* showed how IFP value and steepness of its profile increase with tumor size [129]. Steeper the IFP curve, the harder it becomes to reduce IFP. If that is the case, we expect proangiogenic therapy to halt the convective delivery of large drugs. This scenario can occur in the treatment of large tumors with leaky vessels.

Antiangiogenic agent Cilengitide which exhibit proangiogenic action when used in low doses, is a drug with low toxicity, creating low side effects. It is mostly tried on gliomas as an antiangiogenic agent in high dosed treatment regimens since gliomas are highly vascularized tumors that are a target for antiangiogenic therapy [130]. However, Cilengitide has not shown benefit in clinical outcomes.

Many dose-escalating studies are conducted for Cilengitide, and 2000 mg is shown to be the suitable dose for gliomas [131]. Likewise, greater antitumor activity has been observed among patients having a high dose, 2000 mg, in a randomized phase-II study of recurrent glioblastoma multiforme [132]. It has modest activity in another trial on patients with recurrent glioblastoma, even though the drug reached to therapeutic concentrations [133]. However, in another study, Cilengitide induced normalization is inferred to enhance delivery of temozolomide in the maintenance therapy for Phase I/IIa patients [134]. Cilengitide is observed to have synergistic effects with also radiotherapy. Improvement in outcome is seen when radiation is delivered in normalization window [135]. The effects of radiation are significantly enhanced in the combination of cilengitide and radiotherapy [136].

Even though the clinical results about the antiangiogenic use of Cilengitide are disappointing, proangiogenesis has potential regarding improving physical transport in the tumor microenvironment. By increasing vessel density and leakiness, it may allow low doses of chemotherapy drugs to reach the tumor more efficiently. It has the potential to minimize the side effects of chemotherapy, therefore elongating the therapy [4]. One problem with Cilengitide is its fast clearance from blood, poor blood-brain barrier entrance and high uptake by kidney and liver [137]. All these unfavorable scenarios can be overcome by achieving stable doses of the drug by embedding them into nanoparticles. These effects would be more pronounced for the drugs that depend upon the EPR effect.

6. CONCLUSION

In this thesis, a base mathematical model is built for simulating the nonlinear interaction between tumor growth and angiogenesis during drug therapies. Physical aspects are taken into account when designing the tumor simulator. This novel tumor simulator can calculate the distribution of drugs considering their path from blood vessels to the tumor and back to the lymph system. Their activity on the tumor, as well as the response of the tumor to these drugs, are quantified. Effect of drug combinations, different doses, and treatment schedules are explored for each case to find the most beneficial and remarkable circumstances that determine the outcome of each therapy.

Tumor simulator is adapted to visualize and quantify the effects of normalization in Chapter 4. This adaptation successfully replicates the angiogenesis and resulting vessel distributions commonly observed in real tumors which have a high vessel density in tumor periphery and low vessel density in the tumor center. IFP profile also showed the pressure profile found in actual tumors. A treatment scheduling is proposed for more even distribution of drugs inside the tumor. Finding an optimized schedule and drug dose to achieve normalization, we are able to send the chemotherapy drugs to tumor center. Synergistic effect of normalization with chemotherapy is shown as an enhanced response to chemotherapy. Other major findings include deductions about antiangiogenic drug and IFP interplay and how the dose of antiangiogenic therapy changes the fate of the chemotherapy. By doing trials on the different scheduling of antiangiogenic agents, we found a local minimum in treatment outcome of tumor density four days before application chemotherapy which verified the existence of "the normalization window" suggested by experimental and clinical work in literature. In addition to that IFP is found to be not directly correlated to treatment outcome. Instead, normalization benefit found to be the consequence of the complex interplay between vessels, tumor, and IFP.

Tumor simulator is also used to explore proangiogenic therapies in Chapter 5. This time, different vessel configurations are used to understand the effects of therapies on tumors with different properties. Tumors have the capacity to produce high and low vessel density are simulated. Angiogenesis process is changed in the model to account for the association with its promoter component VEGF. We tried two different drugs to evaluate the effects of proangiogenesis on different transport mechanisms. Small drugs are used to explore proangiogenesis for diffusion-dominated transport of the drugs, and large drugs are used to examine convection dominated transport. The treatment scheduling of combination therapy that yields the best tumor response in terms of tumor shrinkage is proposed as the concurrent therapy of chemotherapy and proangiogenic drugs. Effects of proangiogenesis on treatment response depended on the competition between increased tumor cell proliferation due to enhanced angiogenesis and enhanced drug delivery via increased cell density. Results point out that to tip the balance in favor of tumor shrinkage, fast-acting chemotherapy drugs should be used in the therapy.

REFERENCES

1. Hanahan, D. and R. A. Weinberg, "The hallmarks of cancer", *cell*, Vol. 100, No. 1, pp. 57–70, 2000.

2. Jain, R. K., "Normalization of tumor vasculature: an emerging concept in antiangiogenic therapy", *Science*, Vol. 307, No. 5706, pp. 58–62, 2005.

3. Jain, R. K., "Normalizing tumor microenvironment to treat cancer: bench to bedside to biomarkers", *Journal of Clinical Oncology*, Vol. 31, No. 17, pp. 2205–2218, 2013.

4. Huang, D., H. Lan and F. Liu *et al.*, "Anti-angiogenesis or pro-angiogenesis for cancer treatment: focus on drug distribution", *International Journal of Clinical and Experimental Medicine*, Vol. 8, No. 6, pp. 8369 – 8376, 2016.

5. Knowles, M., *Introduction to the cellular and molecular biology of cancer*, Oxford university press, 2005.

6. Pardee, A. B. and G. S. Stein, *The biology and treatment of cancer: Understanding cancer*, John Wiley & Sons, 2011.

7. King, R. J. B. and M. W. Robins, *Cancer biology*, Pearson Education, 2006.

8. Hanahan, D. and R. A. Weinberg, "Hallmarks of cancer: the next generation", *cell*, Vol. 144, No. 5, pp. 646–674, 2011.

9. Koumoutsakos, P., I. Pivkin and F. Milde, "The fluid mechanics of cancer and its therapy", *Annual review of fluid mechanics*, Vol. 45, 2013.

10. Harris, A. L., "Hypoxia—a key regulatory factor in tumour growth", *Nature Reviews Cancer*, Vol. 2, No. 1, p. 38, 2002.

11. Eales, K., K. Hollinshead and D. Tennant, "Hypoxia and metabolic adaptation of cancer cells", *Oncogenesis*, Vol. 5, No. 1, p. e190, 2016.

12. Vander Heiden, M. G., L. C. Cantley and C. B. Thompson, "Understanding the Warburg effect: the metabolic requirements of cell proliferation", *science*, Vol. 324, No. 5930, pp. 1029–1033, 2009.

13. Jain, R. K., "Antiangiogenesis strategies revisited: from starving tumors to alleviating hypoxia", *Cancer cell*, Vol. 26, No. 5, pp. 605–622, 2014.

14. Folkman, J., "Role of angiogenesis in tumor growth and metastasis", *Seminars in oncology*, Vol. 29, pp. 15–18, Elsevier, 2002.

15. Sivridis, E., A. Giatromanolaki and M. I. Koukourakis, "The vascular network of tumours—what is it not for?", *The Journal of Pathology: A Journal of the Pathological Society of Great Britain and Ireland*, Vol. 201, No. 2, pp. 173–180, 2003.

16. Mittal, K., J. Ebos and B. Rini, "Angiogenesis and the tumor microenvironment: vascular endothelial growth factor and beyond", *Seminars in oncology*, Vol. 41, pp. 235–251, Elsevier, 2014.

17. De Palma, M., D. Biziato and T. V. Petrova, "Microenvironmental regulation of tumour angiogenesis", *Nature Reviews Cancer*, Vol. 17, No. 8, p. 457, 2017.

18. Wu, J., Q. Long and S. Xu *et al.*, "Study of tumor blood perfusion and its variation due to vascular normalization by anti-angiogenic therapy based on 3D angiogenic microvasculature", *Journal of biomechanics*, Vol. 42, No. 6, pp. 712–721, 2009.

19. Lunt, S. J., A. Fyles and R. P. Hill *et al.*, "Interstitial fluid pressure in tumors: therapeutic barrier and biomarker of angiogenesis", *Future Oncology*, Vol. 4, No. 6, pp. 793–802, 2008.

20. Wu, M., H. B. Frieboes and S. R. McDougall *et al.*, "The effect of interstitial pressure on tumor growth: coupling with the blood and lymphatic vascular systems", *Journal of theoretical biology*, Vol. 320, pp. 131–151, 2013.

21. Hassid, Y., E. Furman-Haran and R. Margalit *et al.*, "Noninvasive magnetic resonance imaging of transport and interstitial fluid pressure in ectopic human lung tumors", *Cancer research*, Vol. 66, No. 8, pp. 4159–4166, 2006.

22. Carmeliet, P. and R. K. Jain, "Molecular mechanisms and clinical applications of angiogenesis", *Nature*, Vol. 473, No. 7347, p. 298, 2011.

23. Lin, Z., Q. Zhang and W. Luo, "Angiogenesis inhibitors as therapeutic agents in cancer: challenges and future directions", *European journal of pharmacology*, Vol. 793, pp. 76–81, 2016.

24. Azzi, S., J. K. Hebda and J. Gavard, "Vascular permeability and drug delivery in cancers", *Frontiers in oncology*, Vol. 3, p. 211, 2013.

25. Batchelor, T. T., E. R. Gerstner and K. E. Emblem *et al.*, "Improved tumor oxygenation and survival in glioblastoma patients who show increased blood perfusion after cediranib and chemoradiation", *Proceedings of the national academy of sciences*, Vol. 110, No. 47, pp. 19059–19064, 2013.

26. Viallard, C. and B. Larrivée, "Tumor angiogenesis and vascular normalization: alternative therapeutic targets", *Angiogenesis*, Vol. 20, No. 4, pp. 409–426, 2017.

27. Reynolds, A. R., I. R. Hart and A. R. Watson *et al.*, "Stimulation of tumor growth and angiogenesis by low concentrations of RGD-mimetic integrin inhibitors", *Nature medicine*, Vol. 15, No. 4, p. 392, 2009.

28. Legler, D. F., G. Wiedle and F. P. Ross *et al.*, "Superactivation of integrin (α) v (β) 3 by low antagonist concentrations", .

29. Wong, P.-P., F. Demircioglu and E. Ghazaly *et al.*, "Dual-action combination therapy enhances angiogenesis while reducing tumor growth and spread", *Cancer cell*, Vol. 27, No. 1, pp. 123–137, 2015.

30. Rivera, L. B. and G. Bergers, "Tumor angiogenesis, from foe to friend", *Science*, Vol. 349, No. 6249, pp. 694–695, 2015.

31. Nagy, J. A. and H. F. Dvorak, "Heterogeneity of the tumor vasculature: the need for new tumor blood vessel type-specific targets", *Clinical & experimental metastasis*, Vol. 29, No. 7, pp. 657–662, 2012.

32. Jain, R. K., R. T. Tong and L. L. Munn, "Effect of vascular normalization by antiangiogenic therapy on interstitial hypertension, peritumor edema, and lymphatic metastasis: insights from a mathematical model", *Cancer research*, Vol. 67, No. 6, pp. 2729–2735, 2007.

33. Goh, Y.-M. F., H. L. Kong and C.-H. Wang, "Simulation of the delivery of doxorubicin to hepatoma", *Pharmaceutical Research*, Vol. 18, No. 6, pp. 761–770, 2001.

34. Rofstad, E. K., K. Galappathi and B. S. Mathiesen, "Tumor interstitial fluid pressure—a link between tumor hypoxia, microvascular density, and lymph node metastasis", *Neoplasia*, Vol. 16, No. 7, pp. 586–594, 2014.

35. Tong, R. T., Y. Boucher and S. V. Kozin *et al.*, "Vascular normalization by vascular endothelial growth factor receptor 2 blockade induces a pressure gradient across the vasculature and improves drug penetration in tumors", *Cancer res*, Vol. 64, No. 11, pp. 3731–3736, 2004.

36. Fukumura, D. and R. K. Jain, "Tumor microvasculature and microenvironment: targets for anti-angiogenesis and normalization", *Microvascular research*, Vol. 74, No. 2, pp. 72–84, 2007.

37. Han, B., C. Qu and K. Park *et al.*, "Recapitulation of complex transport and action of drugs at the tumor microenvironment using tumor-microenvironment-on-chip", *Cancer letters*, Vol. 380, No. 1, pp. 319–329, 2016.

38. Michl, P. and T. M. Gress, "Improving drug delivery to pancreatic cancer: breaching the stromal fortress by targeting hyaluronic acid", *Gut*, Vol. 61, No. 10, pp. 1377–1379, 2012.

39. Drasdo, D. and S. Höhme, "A single-cell-based model of tumor growth in vitro: monolayers and spheroids", *Physical biology*, Vol. 2, No. 3, p. 133, 2005.

40. Bauer, A. L., T. L. Jackson and Y. Jiang, "A cell-based model exhibiting branching and anastomosis during tumor-induced angiogenesis", *Biophysical journal*, Vol. 92, No. 9, pp. 3105–3121, 2007.

41. Del Monte, U., "Does the cell number 109 still really fit one gram of tumor tissue?", *Cell Cycle*, Vol. 8, No. 3, pp. 505–506, 2009.

42. Wodarz, D. and N. L. Komarova, *Dynamics of cancer: mathematical foundations of oncology*, World Scientific, 2014.

43. Baish, J. W., P. A. Netti and R. K. Jain, "Transmural coupling of fluid flow in microcirculatory network and interstitium in tumors", *Microvascular research*, Vol. 53, No. 2, pp. 128–141, 1997.

44. Kohandel, M., M. Kardar and M. Milosevic *et al.*, "Dynamics of tumor growth and combination of anti-angiogenic and cytotoxic therapies", *Physics in Medicine and Biology*, Vol. 52, No. 13, p. 3665, 2007.

45. Phipps, C., *Combination of chemotherapy and antiangiogenic therapies: a mathematical modelling approach*, Master's Thesis, University of Waterloo, 2009.

46. Zhang, L., M. Pfister and B. Meibohm, "Concepts and challenges in quantitative

pharmacology and model-based drug development", *The AAPS journal*, Vol. 10, No. 4, pp. 552–559, 2008.

47. Danhof, M., "Systems pharmacology–Towards the modeling of network interactions", *European Journal of Pharmaceutical Sciences*, Vol. 94, pp. 4–14, 2016.

48. Derendorf, H. and B. Meibohm, "Modeling of pharmacokinetic/pharmacodynamic (PK/PD) relationships: concepts and perspectives", *Pharmaceutical research*, Vol. 16, No. 2, pp. 176–185, 1999.

49. Wang, Z., J. D. Butner and V. Cristini *et al.*, "Integrated PK-PD and agent-based modeling in oncology", *Journal of pharmacokinetics and pharmacodynamics*, Vol. 42, No. 2, pp. 179–189, 2015.

50. Schneider, J. B., "Understanding the finite-difference time-domain method", *School of electrical engineering and computer science Washington State University*, 2010.

51. Jain, R. K., "Barriers to drug delivery in solid tumors.", *Scientific American*, Vol. 271, No. 1, p. 58, 1994.

52. Goel, S., A. H.-K. Wong and R. K. Jain, "Vascular normalization as a therapeutic strategy for malignant and nonmalignant disease", *Cold Spring Harbor perspectives in medicine*, Vol. 2, No. 3, p. a006486, 2012.

53. Boucher, Y., L. T. Baxter and R. K. Jain, "Interstitial pressure gradients in tissue-isolated and subcutaneous tumors: implications for therapy", *Cancer research*, Vol. 50, No. 15, pp. 4478–4484, 1990.

54. Boucher, Y. and R. K. Jain, "Microvascular pressure is the principal driving force for interstitial hypertension in solid tumors: implications for vascular collapse", *Cancer research*, Vol. 52, No. 18, pp. 5110–5114, 1992.

55. Netti, P. A., L. T. Baxter and Y. Boucher, "Time-dependent behavior of interstitial fluid pressure in solid tumors: implications for drug delivery", *Cancer Research*, Vol. 55, No. 22, pp. 5451–5458, 1995.

56. Jain, R. K., "Determinants of tumor blood flow: a review", *Cancer research*, Vol. 48, No. 10, pp. 2641–2658, 1988.

57. Chauhan, V. P., T. Stylianopoulos and Y. Boucher *et al.*, "Delivery of molecular and nanoscale medicine to tumors: transport barriers and strategies", *Annual review of chemical and biomolecular engineering*, Vol. 2, pp. 281–298, 2011.

58. Jain, R. K., "Normalizing tumor vasculature with anti-angiogenic therapy: a new paradigm for combination therapy", *Nature medicine*, Vol. 7, No. 9, p. 987, 2001.

59. Carmeliet, P. and R. K. Jain, "Principles and mechanisms of vessel normalization for cancer and other angiogenic diseases", *Nature reviews Drug discovery*, Vol. 10, No. 6, pp. 417–427, 2011.

60. Chauhan, V. P., T. Stylianopoulos and J. D. Martin *et al.*, "Normalization of tumour blood vessels improves the delivery of nanomedicines in a size-dependent manner", *Nature nanotechnology*, Vol. 7, No. 6, pp. 383–388, 2012.

61. Liu, J., S. Liao and B. Diop-Frimpong *et al.*, "TGF-β blockade improves the distribution and efficacy of therapeutics in breast carcinoma by normalizing the tumor stroma", *Proceedings of the National Academy of Sciences*, Vol. 109, No. 41, pp. 16618–16623, 2012.

62. Davis, D., H. R and J. Abbruzzese, "Antiangiogenic cancer therapy", , 2008.

63. Hurwitz, H., L. Fehrenbacher and W. Novotny *et al.*, "Bevacizumab plus irinotecan, fluorouracil, and leucovorin for metastatic colorectal cancer", *New England journal of medicine*, Vol. 350, No. 23, pp. 2335–2342, 2004.

64. Kabbinavar, F., H. I. Hurwitz and L. Fehrenbacher *et al.*, "Phase II, randomized trial comparing bevacizumab plus fluorouracil (FU)/leucovorin (LV) with FU/LV alone in patients with metastatic colorectal cancer", *Journal of Clinical Oncology*, Vol. 21, No. 1, pp. 60–65, 2003.

65. Tebbutt, N. C., K. Wilson and V. J. Gebski *et al.*, "Capecitabine, Bevacizumab, and Mitomycin in First-Line Treatment of Metastatic Colorectal Cancer: Results of the Australasian Gastrointestinal Trials Group Randomized Phase III MAX Study", *Journal of Clinical Oncology*, Vol. 28, No. 19, pp. 3191–3198, 2010, pMID: 20516443.

66. Reck, M., J. von Pawel and P. Zatloukal *et al.*, "Phase III trial of cisplatin plus gemcitabine with either placebo or bevacizumab as first-line therapy for nonsquamous non–small-cell lung cancer: AVAiL", *Journal of Clinical Oncology*, Vol. 27, No. 8, pp. 1227–1234, 2009.

67. Sandler, A., R. Gray and M. C. Perry *et al.*, "Paclitaxel–carboplatin alone or with bevacizumab for non–small-cell lung cancer", *New England Journal of Medicine*, Vol. 355, No. 24, pp. 2542–2550, 2006.

68. Robert, N. J., V. Diéras and J. Glaspy *et al.*, "RIBBON-1: randomized, double-blind, placebo-controlled, phase III trial of chemotherapy with or without bevacizumab for first-line treatment of human epidermal growth factor receptor 2–negative, locally recurrent or metastatic breast cancer", *Journal of Clinical Oncology*, Vol. 29, No. 10, pp. 1252–1260, 2011.

69. Gray, R., S. Bhattacharya and C. Bowden *et al.*, "Independent review of E2100: a phase III trial of bevacizumab plus paclitaxel versus paclitaxel in women with metastatic breast cancer", *Journal of Clinical Oncology*, Vol. 27, No. 30, pp. 4966–4972, 2009.

70. Miles, D. W., A. Chan and L. Y. Dirix *et al.*, "Phase III study of bevacizumab plus docetaxel compared with placebo plus docetaxel for the first-line treatment

of human epidermal growth factor receptor 2–negative metastatic breast cancer", *Journal of Clinical Oncology*, Vol. 28, No. 20, pp. 3239–3247, 2010.

71. Perren, T. J., A. M. Swart and J. Pfisterer *et al.*, "A phase 3 trial of bevacizumab in ovarian cancer", *New England Journal of Medicine*, Vol. 365, No. 26, pp. 2484–2496, 2011.

72. Batchelor, T. T., A. G. Sorensen and E. di Tomaso *et al.*, "AZD2171, a pan-VEGF receptor tyrosine kinase inhibitor, normalizes tumor vasculature and alleviates edema in glioblastoma patients", *Cancer cell*, Vol. 11, No. 1, pp. 83–95, 2007.

73. Winkler, F., S. V. Kozin and R. T. Tong *et al.*, "Kinetics of vascular normalization by VEGFR2 blockade governs brain tumor response to radiation: role of oxygenation, angiopoietin-1, and matrix metalloproteinases", *Cancer cell*, Vol. 6, No. 6, pp. 553–563, 2004.

74. Huang, Y., T. Stylianopoulos and D. G. Duda *et al.*, "Benefits of vascular normalization are dose and time dependent—letter", *Cancer research*, 2013.

75. Ma, J. and D. J. Waxman, "Combination of antiangiogenesis with chemotherapy for more effective cancer treatment", *Molecular cancer therapeutics*, Vol. 7, No. 12, pp. 3670–3684, 2008.

76. McDougall, S. R., A. Anderson and M. Chaplain *et al.*, "Mathematical modelling of flow through vascular networks: implications for tumour-induced angiogenesis and chemotherapy strategies", *Bulletin of mathematical biology*, Vol. 64, No. 4, pp. 673–702, 2002.

77. McDougall, S. R., A. R. Anderson and M. A. Chaplain, "Mathematical modelling of dynamic adaptive tumour-induced angiogenesis: clinical implications and therapeutic targeting strategies", *Journal of theoretical biology*, Vol. 241, No. 3, pp. 564–589, 2006.

78. Soltani, M. and P. Chen, "Numerical modeling of interstitial fluid flow coupled with blood flow through a remodeled solid tumor microvascular network", *PloS one*, Vol. 8, No. 6, p. e67025, 2013.

79. Welter, M. and H. Rieger, "Interstitial fluid flow and drug delivery in vascularized tumors: a computational model", *PloS one*, Vol. 8, No. 8, p. e70395, 2013.

80. Sefidgar, M., M. Soltani and K. Raahemifar *et al.*, "Numerical modeling of drug delivery in a dynamic solid tumor microvasculature", *Microvascular research*, Vol. 99, pp. 43–56, 2015.

81. Benzekry, S., G. Chapuisat and J. Ciccolini *et al.*, "A new mathematical model for optimizing the combination between antiangiogenic and cytotoxic drugs in oncology", *Comptes Rendus Mathematique*, Vol. 350, No. 1-2, pp. 23–28, 2012.

82. Ledzewicz, U. and H. Schättler, "Optimal and suboptimal protocols for a class of mathematical models of tumor anti-angiogenesis", *Journal of Theoretical Biology*, Vol. 252, No. 2, pp. 295–312, 2008.

83. d'Onofrio, A., U. Ledzewicz and H. Maurer *et al.*, "On optimal delivery of combination therapy for tumors", *Mathematical biosciences*, Vol. 222, No. 1, pp. 13–26, 2009.

84. Pinho, S. T. R. d., F. Bacelar and R. F. S. Andrade *et al.*, "A mathematical model for the effect of anti-angiogenic therapy in the treatment of cancer tumours by chemotherapy", *Nonlinear Analysis: Real World Applications*, Vol. 14, No. 1, pp. 815–828, 2013.

85. Panovska, J., H. M. Byrne and P. K. Maini, "A theoretical study of the response of vascular tumours to different types of chemotherapy", *Mathematical and Computer Modelling*, Vol. 47, No. 5, pp. 560–579, 2008.

86. Stephanou, A., S. R. McDougall and A. R. Anderson *et al.*, "Mathematical mod-

elling of flow in 2D and 3D vascular networks: applications to anti-angiogenic and chemotherapeutic drug strategies", *Mathematical and Computer Modelling*, Vol. 41, No. 10, pp. 1137–1156, 2005.

87. Sengupta, S., D. Eavarone and I. Capila *et al.*, "Temporal targeting of tumour cells and neovasculature with a nanoscale delivery system", *Nature*, Vol. 436, No. 7050, pp. 568–572, 2005.

88. Stylianopoulos, T., J. D. Martin and M. Snuderl *et al.*, "Coevolution of solid stress and interstitial fluid pressure in tumors during progression: implications for vascular collapse", *Cancer research*, Vol. 73, No. 13, pp. 3833–3841, 2013.

89. Jain, R. K., "Transport of molecules in the tumor interstitium: a review", *Cancer research*, Vol. 47, No. 12, pp. 3039–3051, 1987.

90. Leu, A. J., D. A. Berk and A. Lymboussaki *et al.*, "Absence of functional lymphatics within a murine sarcoma: a molecular and functional evaluation", *Cancer research*, Vol. 60, No. 16, pp. 4324–4327, 2000.

91. Vleugel, M., R. Bos and P. Van der Groep *et al.*, "Lack of lymphangiogenesis during breast carcinogenesis", *Journal of clinical pathology*, Vol. 57, No. 7, pp. 746–751, 2004.

92. Pluen, A., Y. Boucher and S. Ramanujan *et al.*, "Role of tumor–host interactions in interstitial diffusion of macromolecules: cranial vs. subcutaneous tumors", *Proceedings of the National Academy of Sciences*, Vol. 98, No. 8, pp. 4628–4633, 2001.

93. Reddy, S. T., D. A. Berk and R. K. Jain *et al.*, "A sensitive in vivo model for quantifying interstitial convective transport of injected macromolecules and nanoparticles", *Journal of applied physiology*, Vol. 101, No. 4, pp. 1162–1169, 2006.

94. Curry, F., "Mechanics and thermodynamics of transcapillary exchange", *Hand-*

book of physiology, Vol. 4, No. part 1, pp. 309–374, 1984.

95. Wu, N. Z., D. Da and T. L. Rudoll *et al.*, "Increased microvascular permeability contributes to preferential accumulation of Stealth liposomes in tumor tissue", *Cancer research*, Vol. 53, No. 16, pp. 3765–3770, 1993.

96. Laginha, K. M., S. Verwoert and G. J. Charrois *et al.*, "Determination of doxorubicin levels in whole tumor and tumor nuclei in murine breast cancer tumors", *Clinical cancer research*, Vol. 11, No. 19, pp. 6944–6949, 2005.

97. Gabizon, A., R. Catane and B. Uziely *et al.*, "Prolonged circulation time and enhanced accumulation in malignant exudates of doxorubicin encapsulated in polyethylene-glycol coated liposomes", *Cancer research*, Vol. 54, No. 4, pp. 987–992, 1994.

98. Graff, B., Y. Kvinnsland and A. Skretting *et al.*, "Intratumour heterogeneity in the uptake of macromolecular therapeutic agents in human melanoma xenografts", *British journal of cancer*, Vol. 88, No. 2, pp. 291–297, 2003.

99. Cabral, H., Y. Matsumoto and K. Mizuno *et al.*, "Accumulation of sub-100 nm polymeric micelles in poorly permeable tumours depends on size", *Nature nanotechnology*, Vol. 6, No. 12, pp. 815–823, 2011.

100. Lee, H., B. Hoang and H. Fonge *et al.*, "In vivo distribution of polymeric nanoparticles at the whole-body, tumor, and cellular levels", *Pharmaceutical research*, Vol. 27, No. 11, pp. 2343–2355, 2010.

101. Karathanasis, E., L. Chan and L. Karumbaiah *et al.*, "Tumor vascular permeability to a nanoprobe correlates to tumor-specific expression levels of angiogenic markers", *PLoS One*, Vol. 4, No. 6, p. e5843, 2009.

102. Stapleton, S., M. Milosevic and I. F. Tannock *et al.*, "The intra-tumoral relationship between microcirculation, interstitial fluid pressure and liposome accumula-

tion", *Journal of Controlled Release*, Vol. 211, pp. 163–170, 2015.

103. Rygh, C. B., S. Qin and J. W. Seo *et al.*, "Longitudinal investigation of permeability and distribution of macromolecules in mouse malignant transformation using PET", *Clinical Cancer Research*, Vol. 17, No. 3, pp. 550–559, 2011.

104. Tailor, T. D., G. Hanna and P. S. Yarmolenko *et al.*, "Effect of pazopanib on tumor microenvironment and liposome delivery", *Molecular cancer therapeutics*, Vol. 9, No. 6, pp. 1798–1808, 2010.

105. Seynhaeve, A. L., S. Hoving and D. Schipper *et al.*, "Tumor necrosis factor α mediates homogeneous distribution of liposomes in murine melanoma that contributes to a better tumor response", *Cancer research*, Vol. 67, No. 19, pp. 9455–9462, 2007.

106. Ekdawi, S. N., J. M. Stewart and M. Dunne *et al.*, "Spatial and temporal mapping of heterogeneity in liposome uptake and microvascular distribution in an orthotopic tumor xenograft model", *Journal of Controlled Release*, Vol. 207, pp. 101–111, 2015.

107. Theek, B., F. Gremse and S. Kunjachan *et al.*, "Characterizing EPR-mediated passive drug targeting using contrast-enhanced functional ultrasound imaging", *Journal of controlled release*, Vol. 182, pp. 83–89, 2014.

108. Stylianopoulos, T. and R. K. Jain, "Combining two strategies to improve perfusion and drug delivery in solid tumors", *Proceedings of the National Academy of Sciences*, Vol. 110, No. 46, pp. 18632–18637, 2013.

109. Ozturk, D., S. Yonucu and D. Yilmaz *et al.*, "Influence of vascular normalization on interstitial flow and delivery of liposomes in tumors", *Physics in medicine and biology*, Vol. 60, No. 4, p. 1477, 2015.

110. Patel, K. J., O. Trédan and I. F. Tannock, "Distribution of the anticancer drugs

doxorubicin, mitoxantrone and topotecan in tumors and normal tissues", *Cancer chemotherapy and pharmacology*, Vol. 72, No. 1, pp. 127–138, 2013.

111. Kim, J. J. and I. F. Tannock, "Repopulation of cancer cells during therapy: an important cause of treatment failure", *Nature Reviews Cancer*, Vol. 5, No. 7, pp. 516–525, 2005.

112. Cogger, V. C., I. M. Arias and A. Warren *et al.*, "The response of fenestrations, actin, and caveolin-1 to vascular endothelial growth factor in SK Hep1 cells", *American Journal of Physiology-Gastrointestinal and Liver Physiology*, Vol. 295, No. 1, pp. G137–G145, 2008.

113. Esser, S., K. Wolburg and H. Wolburg *et al.*, "Vascular endothelial growth factor induces endothelial fenestrations in vitro", *The Journal of cell biology*, Vol. 140, No. 4, pp. 947–959, 1998.

114. Esser, S., M. G. Lampugnani and M. Corada *et al.*, "Vascular endothelial growth factor induces VE-cadherin tyrosine phosphorylation in endothelial cells", *Journal of cell science*, Vol. 111, No. 13, pp. 1853–1865, 1998.

115. Cully, M., "Cancer: Tumour vessel normalization takes centre stage", *Nature Reviews Drug Discovery*, Vol. 16, No. 2, p. 87, 2017.

116. Hernández-Agudo, E., T. Mondejar and M. L. Soto-Montenegro *et al.*, "Monitoring vascular normalization induced by antiangiogenic treatment with 18F-fluoromisonidazole-PET", *Molecular oncology*, Vol. 10, No. 5, pp. 704–718, 2016.

117. Miller, L. M., J. M. Pritchard and S. J. Macdonald, "Emergence of Small-Molecule Non-RGD-Mimetic Inhibitors for RGD Integrins: Miniperspective", *Journal of Medicinal Chemistry*, Vol. 60, No. 8, pp. 3241–3251, 2017.

118. Mas-Moruno, C., F. Rechenmacher and H. Kessler, "Cilengitide: the first anti-angiogenic small molecule drug candidate. Design, synthesis and clinical evalua-

tion", *Anti-Cancer Agents in Medicinal Chemistry (Formerly Current Medicinal Chemistry-Anti-Cancer Agents)*, Vol. 10, No. 10, pp. 753–768, 2010.

119. Demircioglu, F. and K. Hodivala-Dilke, "$\alpha v\beta 3$ Integrin and tumour blood vessels-learning from the past to shape the future", *Current Opinion in Cell Biology*, Vol. 42, pp. 121 – 127, 2016, cell dynamics.

120. d'Onofrio, A. and A. Gandolfi, "Chemotherapy of vascularised tumours: role of vessel density and the effect of vascular "pruning"", *Journal of theoretical biology*, Vol. 264, No. 2, pp. 253–265, 2010.

121. Hubbard, M. E., M. Jove and P. M. Loadman *et al.*, "Drug delivery in a tumour cord model: a computational simulation", *Royal Society open science*, Vol. 4, No. 5, p. 170014, 2017.

122. Stylianopoulos, T., L. L. Munn and R. K. Jain, "Reengineering the Physical Microenvironment of Tumors to Improve Drug Delivery and Efficacy: From Mathematical Modeling to Bench to Bedside", *Trends in cancer*, 2018.

123. Yonucu, S., D. Yilmaz and C. Phipps, "Quantifying the effects of antiangiogenic and chemotherapy drug combinations on drug delivery and treatment efficacy", *PLOS Computational Biology*, Vol. 13, No. 9, 09 2017.

124. Weidner, N., "Chapter 14 Measuring Intratumoral Microvessel Density", *Angiogenesis: In Vivo Systems, Part A*, Vol. 444 of *Methods in Enzymology*, pp. 305 – 323, Academic Press, 2008.

125. Powathil, G. G., "Modeling of Brain Tumors: Effects of Microenvironment and Associated Therapeutic Strategies", *University of Waterloo*, 2009.

126. Heldin, C.-H., K. Rubin, K. Pietras and A. Östman, "High interstitial fluid pressure—an obstacle in cancer therapy", *Nature Reviews Cancer*, Vol. 4, No. 10, p. 806, 2004.

127. Hasan, J., R. Byers and G. C. Jayson, "Intra-tumoural microvessel density in human solid tumours", *British Journal of Cancer*, Vol. 86, No. 10, pp. 1566–1577, 2002.

128. McCormack, D. R., A. J. Walsh and W. Sit *et al.*, "In vivo hyperspectral imaging of microvessel response to trastuzumab treatment in breast cancer xenografts", *Biomed. Opt. Express*, Vol. 5, No. 7, pp. 2247–2261, Jul 2014.

129. Ozturk, D., S. Yonucu and D. Yilmaz *et al.*, "Influence of vascular normalization on interstitial flow and delivery of liposomes in tumors", *Physics in Medicine & Biology*, Vol. 60, No. 4, p. 1477.

130. Keunen, O., M. Johansson and A. Oudin *et al.*, "Anti-VEGF treatment reduces blood supply and increases tumor cell invasion in glioblastoma", *Proceedings of the National Academy of Sciences*, Vol. 108, No. 9, pp. 3749–3754, 2011.

131. Nabors, L. B., T. Mikkelsen and M. E. Hegi *et al.*, "A safety run-in and randomized phase 2 study of cilengitide combined with chemoradiation for newly diagnosed glioblastoma (NABTT 0306)", *Cancer*, Vol. 118, No. 22, pp. 5601–5607.

132. Reardon, D. A., K. L. Fink and T. Mikkelsen *et al.*, "Randomized phase II study of cilengitide, an integrin-targeting arginine-glycine-aspartic acid peptide, in recurrent glioblastoma multiforme", *Journal of clinical oncology*, Vol. 26, No. 34, pp. 5610–5617, 2008.

133. Gilbert, M. R., J. Kuhn and K. R. Lamborn *et al.*, "Cilengitide in patients with recurrent glioblastoma: the results of NABTC 03-02, a phase II trial with measures of treatment delivery", *Journal of neuro-oncology*, Vol. 106, No. 1, pp. 147–153, 2012.

134. Stupp, R., M. E. Hegi and B. Neyns *et al.*, "Phase I/IIa study of cilengitide and temozolomide with concomitant radiotherapy followed by cilengitide and temo-

zolomide maintenance therapy in patients with newly diagnosed glioblastoma", *Journal of clinical oncology*, Vol. 28, No. 16, pp. 2712–2718, 2010.

135. Elmghirbi, R., T. N. Nagaraja and S. L. Brown *et al.*, "In vivo hyperspectral imaging of microvessel response to trastuzumab treatment in breast cancer xenografts", *Radiation Research*, Vol. 187, No. 1, pp. 79–88, 2016.

136. Mikkelsen, T., C. Brodie and S. Finniss *et al.*, "Radiation sensitization of glioblastoma by cilengitide has unanticipated schedule-dependency", *International Journal of Cancer*, 2009.

137. Zhao, Y.-Z., Q. Lin and H. L. Wong *et al.*, "Glioma-targeted therapy using Cilengitide nanoparticles combined with UTMD enhanced delivery", *Journal of Controlled Release*, Vol. 224, pp. 112 – 125, 2016.